



Universidad Autónoma
de Madrid

Biblos-e Archivo
Repositorio Institucional UAM

Repositorio Institucional de la Universidad Autónoma de Madrid

<https://repositorio.uam.es>

Esta es la **versión de autor** del artículo publicado en:

This is an **author produced version** of a paper published in:

Journal of Environmental Chemical Engineering 9.6 (2021): 106419

DOI: <https://doi.org/10.1016/j.jece.2021.106419>

Copyright: © 2021 Elsevier Ltd. This manuscript version is made available under the CC-BY-NC-ND 4.0 licence <http://creativecommons.org/licenses/by-nc-nd/4.0/>

El acceso a la versión del editor puede requerir la suscripción del recurso

Access to the published version may require subscription

Enhancement of activity and selectivity to nitrogen in catalytic nitrate reduction by use of conductive carbon catalytic supports and control of hydrogen mass transfer regime

D.T. González, A. Marí, J.A. Baeza, L. Calvo*, M.A. Gilarranz

Departamento de Ingeniería Química, C/Francisco Tomás y Valiente 7, Universidad Autónoma de Madrid, 28049 Madrid, Spain

*corresponding author e-mail: luisa.calvo@uam.es

Abstract

Carbon materials with different structural properties (activated carbon, carbon nanofibers, reduced graphene oxide, graphite, and carbon black) were used as supports of Pd-Cu (5 wt. %) catalysts for the catalytic reduction of NO_3^- in batch reactors. In general, those catalyst with smaller metal nanoparticles and carbon supports with higher specific surface area were more active, although remarkable activity was also observed for catalysts with relatively large nanoparticles and conductive supports. Conductivity of carbon supports also contributed to a lower selectivity to NH_4^+ , which can be ascribed to higher charge transfer between metal and support reducing activation of intermediate species. The decrease of H_2 feed into the reaction system resulted in external (gas-liquid) mass transfer constrains, as evidenced by the parameters describing control regime, and led to diminished NH_4^+ selectivity, particularly in the case of catalysts with conductive supports. Approaches combining control of mass transfer regime and conductive carbon catalytic supports can be useful to enhance selectivity to N_2 , which is a major challenge in catalytic NO_3^- reduction.

Keywords

NO_3^- reduction, carbon, conductive supports, Pd-Cu catalysts, mass transfer limitations

1. Introduction

Catalytic reduction of NO_3^- was firstly reported by Vorlop et al. [1], since then, it has attracted much attention as an interesting alternative for drinking water treatment. The process consists in the catalytic reduction of NO_3^- using H_2 (or a source of H_2) at temperatures and pressures near ambient ones. The relatively low operation costs and the absence of post-treatment are among the main advantages of this process compared with traditional physicochemical and biological treatments. The most accepted mechanism for the catalytic reduction of NO_3^- proposes firstly NO_3^- reduction to NO_2^- , and secondly NO_2^- reduction to N_2 or NH_4^+ , through N-containing intermediate species adsorbed on catalysts surface [2]. EU regulation establishes 50, 0.1 and 0.5 mg/L as limits in drinking water for NO_3^- , NO_2^- and NH_4^+ , respectively [3].

The proper control of the selectivity to undesired products (i.e. NO_2^- , NH_4^+) is still a challenge. Several variables influencing the reduction mechanism and the selectivity to NH_4^+ such as the type of reactor, pH, catalysts, and operating conditions, among others, are known [2, 4]. Different metallic phases and supports have been studied to better understand catalyst influence on selectivity. Regarding the metallic phase, Rh, Pt and Pd are widely used [4], being the latter one of the most used noble metals due to its good ability to reduce NO_3^- . A second metal is commonly used as it promotes in the first step the reduction from NO_3^- to NO_2^- through a redox cycle involving Pd and H_2 . Different promoter metals such as Sn, In or Cu are among the most used. [2]

A great variety of catalyst supports including zeolites, titania, ceria, alumina, clays and carbon materials, especially activated carbon, have been used in catalytic NO_3^- reduction [5]. Carbon materials are versatile and present noticeable features such as inertness, hydrothermal stability, and facility to recover metallic phase, among others [6]. Moreover, their physical and chemical composition can be tailored through different

methods. Carbon materials are found in a great number of different structures leading to different properties, which makes them suitable candidates to study the role of supports in catalytic activity and selectivity. Activated carbon has been widely used as carbon support in catalytic NO_3^- reduction due to their large surface area, however, some authors [5] have reported that surface area not always has a significant influence on activity. Carbon supports with more ordered structure, such as graphite (G), carbon nanofibers (CNF) or carbon blacks, have been less studied probably due to their lower surface area. Nevertheless, these supports with a more ordered structure could facilitate charge delocalization and transfer, and could have an impact on activity and/or selectivity given the redox nature of the reactions involved.

Another crucial variable influencing activity and selectivity is the availability of reducing agent at catalytic centers. A high concentration of H_2 in the reactor system can lead to an increase in NO_3^- and NO_2^- conversion rate, but also an increase in selectivity to NH_4^+ . High H:N ratios at active sites lead to overreduction of the N-containing intermediate species adsorbed, since N-H bonds formation is favored compared to N-N bonds [7]. In a recent work [8], we have reported on the relevance of establishing operating conditions leading to mass transfer limitations for H_2 in fixed bed reactors as an approach to control selectivity to NH_4^+ .

In the present work, carbon materials with different structural ordering have been studied as supports for bimetallic Pd-Cu metallic phase and in batch NO_3^- reduction. Moreover, the influence of H_2 availability in the reaction system was studied, and the parameters describing H_2 transfer in the system and their links with catalyst performance were assessed.

2. Experimental

2.1 Materials

PdCl_2 (> 99.9 %), $\text{CuCl}_2 \cdot 2\text{H}_2\text{O}$ (> 99.9 %), graphite (G), graphitized carbon nanofibers (CNF) and 2,6-Pyridinedicarboxylic acid (> 99.5 %) were provided by Sigma-Aldrich. NaNO_3 (99 %), NaNO_2 (98 %), NH_4Cl (99.5 %), Na_2CO_3 (99 %), NaHCO_3 (99.5 %) and HNO_3 (65 %) were supplied by Panreac. H_2 (> 99.999 %) and CO_2 (> 99.99 %) were supplied by Nippon gases. Reduced graphene oxide (rGO), activated carbon (AC), and carbon blacks ENSACO250G (ENS250) and ENSACO350G (ENS350) were purchased from Graphenea, Norit, and Timcal, respectively.

2.2. Catalysts preparation and characterization

Bimetallic catalysts (5 wt %) were prepared using Pd and Cu (2:1 wt %) as metallic phase and carbon materials as supports. The catalysts were prepared by successive wet impregnation. A PdCl_2 solution (4 mL) in 0.1 M HCl was mixed with 0.4 g of carbon support in a rotary-evaporator at 70°C, 200 rpm and 150 mbar until dryness. Then, this step was repeated with a $\text{CuCl}_2 \cdot 2\text{H}_2\text{O}$ (4 mL) solution. The catalysts were left overnight in an oven at 60 °C and, finally, calcined at 200 °C for 2 h and reduced at 200 °C under H_2 flow (25 N mL/min). The supports were characterized by N_2 adsorption-desorption at -196 °C (Tristar II, Micromeritics); XRD (X-pert PRO Theta/2Theta, Panalytical), where the stacking height (L_c) and crystallite size (L_a) parameters were calculated using Scherrer equation from (002) and (100) peaks.

Resistivity measurements were performed using a 4-point probe at different pressures (0-180 MPa). The catalysts were characterized by TEM (JEOL JEM 2100 with EDS, Oxford instruments). TEM micrographs were used to analyze nanoparticle mean diameter, standard deviation, and frequency histograms. At least 200 nanoparticles from different micrographs were counted for each catalyst.

2.3 Adsorption and catalytic runs

NO_3^- adsorption tests were carried out with all the carbon supports in a jacketed glass reactor at 30 °C and atmospheric pressure. 30-60 mg of support was placed into the reactor together with 150 mL of a 100 mg/L NO_3^- solution under stirring (800 rpm) for 4 h. Catalytic runs were also carried out at 30 °C and atmospheric pressure using the same experimental setup described for the adsorption tests. A typical run started with 140 mL of water mixed with a known amount of catalysts (30-60 mg) and subjected to vigorous stirring (800 rpm) under H_2 (50 N mL/min) and CO_2 (50 N mL/min) flows for 30 min. Then a concentrated solution of NO_3^- (10 mL) was added to reach the desired initial concentration (20-100 mg/L) at $t = 0$. The liquid samples (1 mL) were collected and filtered (PTFE filter, pore size 0.22 μm) before their analysis. Liquid chromatography (Metrohm 882 Compact IC plus anion and cation) with a Metrosep C4 column using a 1.7 mM HNO_3^- + 0.7 mM 2,6-Pyridinedicarboxylic acid eluent (0.9 mL/min) was used for cation separation. A Metrosep A Supp 5 column and 3.2 mM Na_2CO_3 + 1 mM NaHCO_3 eluent (0.7 mL/min) was used for anion separation. NO_3^- conversion and selectivity to NO_2^- and NH_4^+ were calculated according to Eqs. 3, 4 and 5, respectively, where $n_{A, t=0}$ is the initial amount of compound A (mol) and $n_{A, t}$ is the amount of compound A (mol) at time t (min).

$$X_{\text{NO}_3^-}(\%) = \frac{n_{\text{NO}_3^-, t=0} - n_{\text{NO}_3^-, t}}{n_{\text{NO}_3^-, t=0}} \cdot 100 \quad (3)$$

$$S_{\text{NO}_2^-}(\%) = \frac{n_{\text{NO}_2^-, t}}{n_{\text{NO}_3^-, t=0} - n_{\text{NO}_3^-, t}} \cdot 100 \quad (4)$$

$$S_{\text{NH}_4^+}(\%) = \frac{n_{\text{NH}_4^+, t}}{n_{\text{NO}_3^-, t=0} - n_{\text{NO}_3^-, t}} \cdot 100 \quad (5)$$

2.4 Mass transfer regime study

With the aim of assessing the behavior of the catalysts at different H₂ flow conditions, a mass transfer regime study was carried out. The external mass transfer was assessed through the calculation of the Carberry number for the gas-liquid (Ca_{G-L}) and liquid-solid (Ca_{L-S}) mass transfer, respectively, according to Eqs. 6 and 7.

$$Ca_{G-L} = \frac{R(i)_{obs}}{K_L a_v \cdot C_i^*} \quad (6)$$

$$Ca_{L-S} = \frac{R(i)_{obs}}{K_S a_p \cdot C_i^*} \quad (7)$$

where $R(i)_{obs}$ (mmol/L·s) corresponds to the observed reaction rate for H₂ transfer and H₂ and NO₃⁻ for Ca_{G-L} and Ca_{L-S} , respectively. $R(NO_3^-)_{obs}$ could not be calculated strictly as initial rate because for some catalysts the effect of nitrate adsorption was significant at short reaction times. Reaction rate was calculated up to ca. 50% conversion as long as a linear trend was maintained. The denominator in both Eqs. 6 and 7 corresponds to the maximum external mass transfer rate ($R(i)_{max}$), being $K_L a_v$ (s⁻¹) and $K_S a_p$ (s⁻¹) the gas-liquid and liquid-solid mass transfer coefficients and C_i^* the concentration of H₂ or NO₃⁻ (mmol/L) in the liquid phase or in the solid surface at equilibrium, assuming a maximum gradient of concentration across the boundary layer. In the case of H₂ the concentration was calculated by Henry's Law (Eq. 8). Mass transfer limitations can be discarded when Carberry number is lower than 0.1.

$$C_i = H \cdot P_i \quad (8)$$

where C_i corresponds to the H_2 concentration at equilibrium, H is the Henry's constant for the H_2/H_2O system and P_i is the partial pressure of H_2 in the medium. $K_L a_v$ was calculated from the dimensional correlation proposed by Yagi and Yoshida [9] (Eq. 9-13)

$$Sh = 0.06 \cdot Re^{1.5} \cdot Fr^{0.19} \cdot Sc^{0.5} \cdot \left(\frac{\mu_L \cdot u_g}{\sigma_L} \right)^{0.6} \cdot \left(\frac{d_I \cdot N}{u_g} \right)^{0.32} \quad (9)$$

$$Sh = \frac{K_L a_v \cdot d_I^2}{D_{mi}} \quad (10)$$

$$Re = \frac{d_I^2 \cdot N \cdot \rho_L}{\mu_L} \quad (11)$$

$$Fr = \frac{d_I \cdot N^2}{g} \quad (12)$$

$$Sc = \frac{\mu_L}{\rho_L \cdot D_{mi}} \quad (13)$$

where Sh , Re , Fr and Sc are the Sherwood, Reynolds, Froude, and Schmidt numbers, respectively. μ_L is the water viscosity (kg/m·s), u_g is the gas surface velocity (m/s), σ_L is the surface tension of water (kg/s), d_I is the magnetic stirrer diameter (m), ρ_L is the water density (kg/m³) and N is agitation velocity (s⁻¹), g is the gravity (m/s²) and D_{mi} is the molecular diffusivity calculated from Wilke-Chang equation [10] (Eq. 14)

$$D_{mi} = 7.4 \cdot 10^{-8} \cdot \frac{(\alpha \cdot M_w)^{0.5} \cdot T}{\mu_L \cdot V_i^{0.6}} \quad (14)$$

where α is the association coefficient (2.6 for water), M_w is the molecular mass of solvent (g/mol), T is the temperature (K), μ_L is solvent viscosity (g/cm·s) and V_i is the molar volume at the normal boiling point (cm³/mol)

$K_S a_p$ was estimated through Ranz and Marshall correlation [11] (Eq. 15) and Sherwood number (Eq. 16)

$$Sh = 2 + 0.6 \cdot Re^{1/2} \cdot Sc^{1/3} \quad (15)$$

$$Sh = \frac{k_s \cdot d_p}{D_{mi}} \quad (16)$$

where d_p corresponds to particle diameter and a_p can be expressed for spherical particles as $6/d_p$

Weisz-Prater criterion was used, as proposed by Lee [12] (Eq. 17) in order to analyze internal diffusion limitations. In first-order reactions using spherical catalysts, mass transfer limitations can be discarded when the Weisz-Prater module is lower than 1. First order kinetic constant was calculated from $\ln[\text{NO}_3^-]$ vs t plot. Different authors reported pseudo-first or first order kinetics in the catalytic reduction of nitrate using bimetallic Pd-based catalysts [13-15]

$$(\Phi_s)_i = \frac{R(i)_{obs} \cdot (d_p/6)^2}{C_i^* \cdot De_i} \quad (17)$$

Where De_i is the effective diffusivity of the compound i inside catalyst pores (cm^2/s). This was estimated, using Butt criteria, as 10 % of the molecular diffusivity in the liquid medium when tortuosity is unknown [16].

3. Results and discussion

3.1 Support and catalysts characterization

Table 1 shows the BET specific surface area (SSA_{BET}) and meso and micropore volume of the supports. Different SSA_{BET} from very low values (G, CNF) to relatively high (AC, ENS350) were obtained. Likewise, different pore volumes, from very low (G, CNF and ENS250) to relatively high (rGO, AC and ENS350) were observed.

Table 1. BET specific surface area, meso and micropore volume of the supports

Support	SSA_{BET} (m ² /g)	Mesopore volume (cm ³ /g)	Micropore volume (cm ³ /g)
G	2	0.04	0.003
CNF	4	0.06	0.005
rGO	86	0.59	0.12
AC	1210	0.38	0.53
ENS250	65	0.09	<0.001
ENS350	770	0.74	0.12

Figure 1 shows the X-ray diffractograms for the supports analyzed. All the patterns exhibited a diffraction peak at ca. 26° corresponding to the reflection plane of aromatic layers (002). This peak is related to the graphitization degree of carbon materials, being the orientation of the aromatic layers higher as the peak (002) gets narrower and more intense [17]. On the other hand, the samples showed another peak close to 42°, corresponding to the reflection plane (100) of aromatic layers. In the case of G, the plane (002) was related to the orientation of the aromatic layers in a 3-D arrangement, whereas the plane (100) was attributed to the degree of condensation of the aromatic carbon rings, thus, the peak (100) becomes narrower and higher as the size of the aromatic layer domains grows [18].

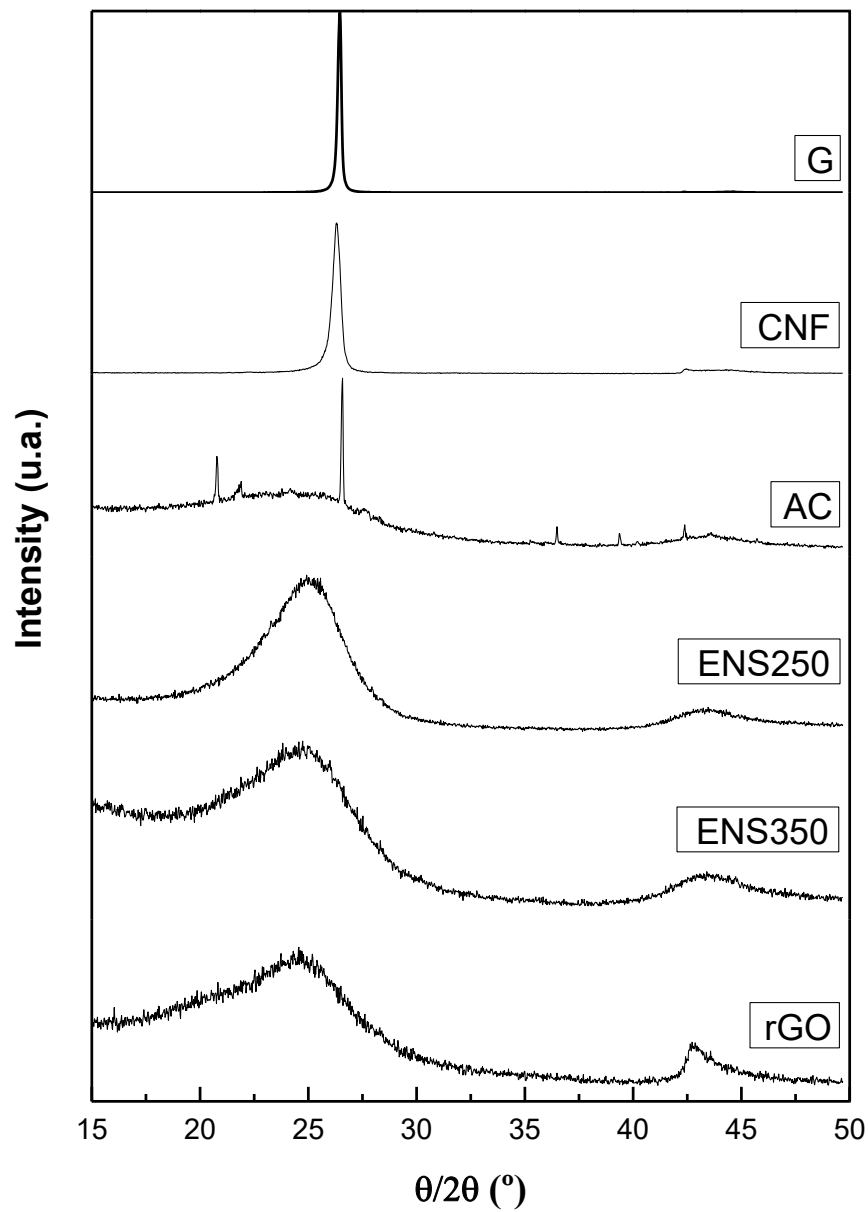


Figure 1. X-ray diffractograms for the carbon materials analyzed.

Table 2 represents L_c and L_a values for the different carbon materials. L_c values show that G and CNF are the supports with the highest stacking height, whereas the other supports are in a range of relatively low stacking height and small crystallite size. These results are good in agreement with Figure 1, where G and CNF show the sharpest (002) peaks among

the supports. Regarding to L_a , it was calculated only for the supports exhibiting a diffraction peak (001) clearly resolved. OGR, the most amorphous support, showed the highest value.

Table 2. L_c and L_a values for the different carbon materials studied.

Support	L_c (nm)	L_a (nm)
G	41.5	-
CNF	18.3	-
AC	1.4	-
ENS250	1.7	3.1
ENS350	0.6	2.5
rGO	0.7	8.2

Figure 2 represents the electrical resistivity vs pressure for the supports tested. It can be observed that increasing pressure from 0 to 37 MPa produced a decrease in resistivity due to sample compaction. In general, increasing pressure from 37 to 185 MPa did not lead to significant changes in resistivity, except for rGO, which can be ascribed to the very low density of the material (ca. 0.05 g/cm³), which results in ability for compaction. CNF and ENS350 are the most conductive supports and rGO is the less conductive, whereas AC, G and ENS250 showed an intermediate behavior. These measurements offered a reasonable approximation to the ability of the supports to transfer charge, but it must be noted that resistivity measurements were made on a carbon disk, and resistivity values may differ at real reaction conditions.

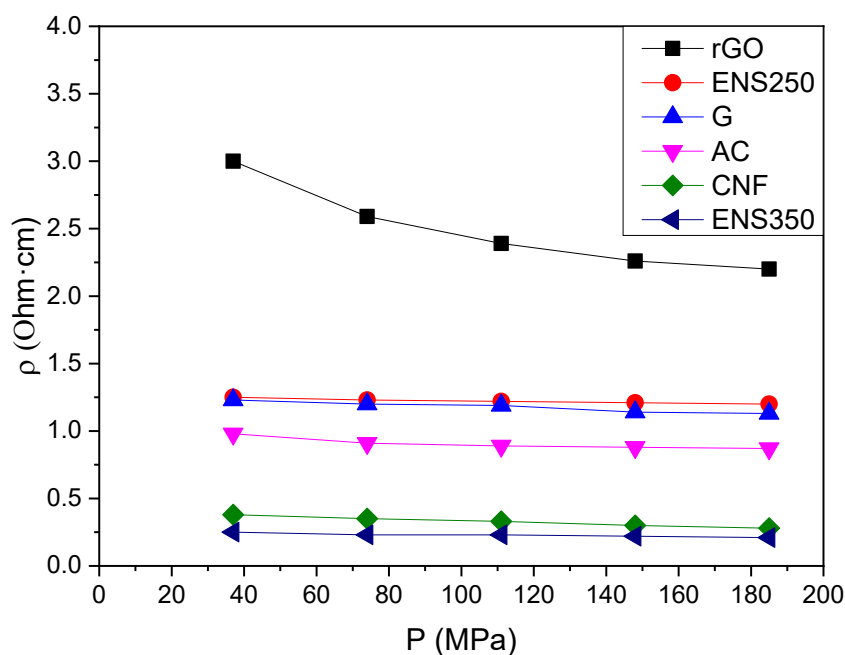
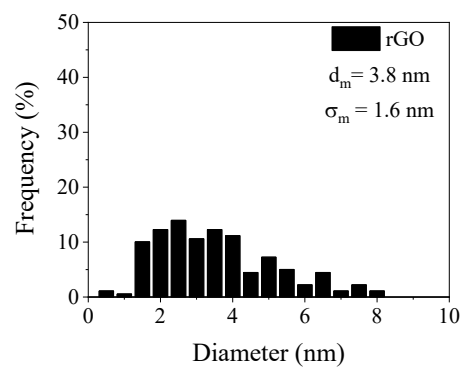
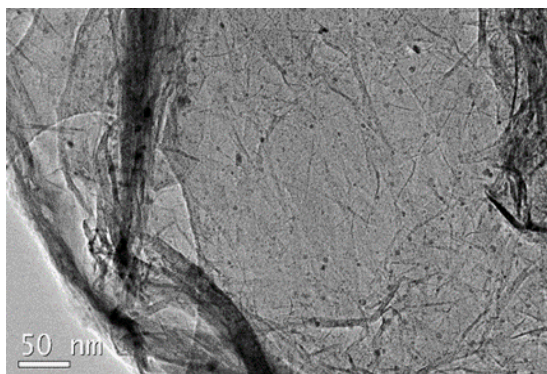
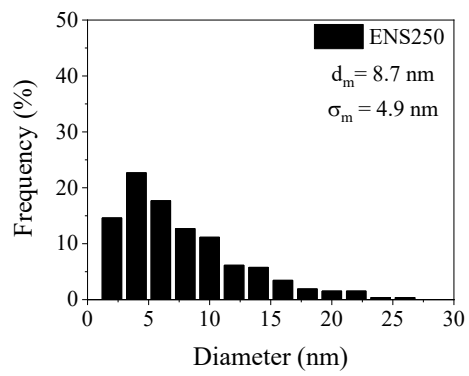
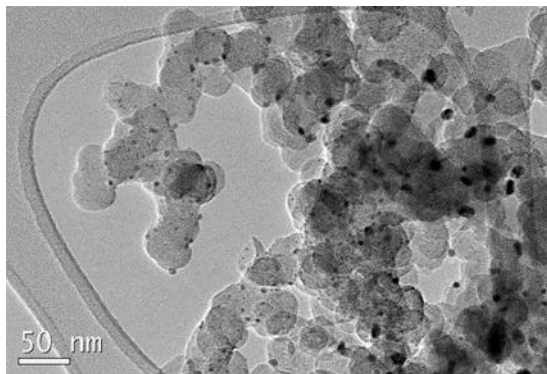
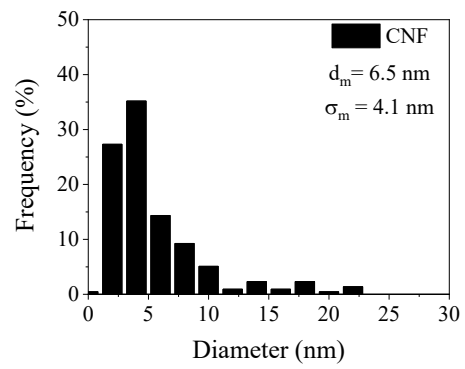
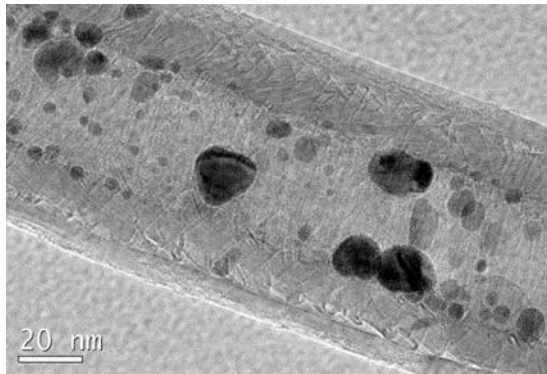
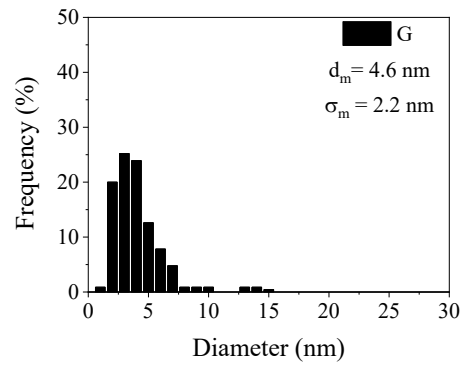
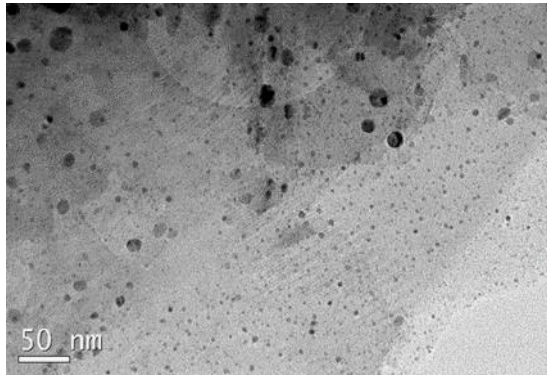


Figure 2. Resistivity vs Pressure curves for the supports tested.

Figure 3 shows representative TEM images showing dispersion of the metal phase, frequency histograms, nanoparticle mean size and standard deviation for all the catalyst prepared. Nanoparticle mean size and standard deviation were in a range from 1.4 to 8.7 nm and 0.4 to 4.9 nm, respectively. Pd-Cu/ENS350 and Pd-Cu/AC show both lower mean size and standard deviation, leading to well-dispersed small particles. ENS350 and AC supports present high specific surface area that facilitates metal dispersion. A higher amount of surface oxygen groups contributing to the formation of metal nuclei and limiting growth can also be expected in the case of AC [19]. On the other hand, Pd-Cu/CNF, and Pd-Cu/ENS250 show larger nanoparticle mean size and higher presence of larger particles (>10 nm) than the other catalysts.



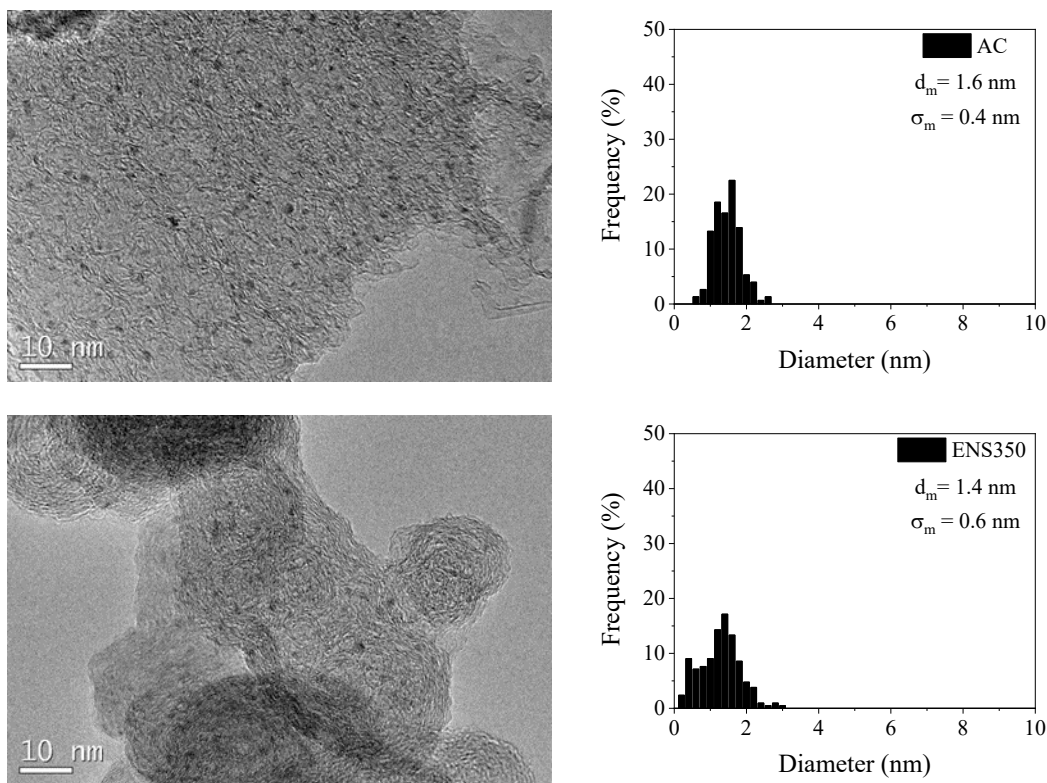


Figure 3. TEM images and nanoparticle size histograms for the catalysts prepared

3.2 Reaction tests

Previous to reaction tests, NO_3^- adsorption experiments using supports without metallic phase, both in the absence and the presence of H_2 and CO_2 , were carried out. The uptake of NO_3^- ranged between 1 and 16 %. Traces of NO_2^- and NH_4^+ were detected during the adsorption experiments when rGO, AC, ENS250 and ENS350 supports were tested, which indicates that supports barely contributed to NO_3^- conversion. No traces of reaction products were detected for NFC and G supports.

Figure 4 depicts NO_3^- conversion vs time curves for all the catalysts tested using a NO_3^- initial concentration of 100 mg/L. After 4 h, NO_3^- conversion was in a range from 32 to 100 %, being the catalysts supported on ENS350 and AC the most active ones. These supports presented the highest specific surface area (770-1210 m^2/g) among the set studied. Those catalysts with supports of low specific surface area, such as rGO, G or

CNF (2-86 m²/g), did not reach total conversion, except the one supported on ENS250 (65 m²/g), whose activity was slightly lower than that observed for Pd-Cu/AC. Yoshinaga et al. [20] studied the catalytic NO₃⁻ reduction using Pd-Cu supported on different materials such as alumina, zirconia, silica and activated carbon, reporting that high surface areas of the catalysts support led to high NO₃⁻ conversion. However, Soares et al. [5] found no significant effect of specific surface area on activity when they studied the performance of Pd-Cu bimetallic catalysts supported in several materials such as titania, AC, carbon nanotubes, manganese oxide, silica, ceria, etc.

As discussed above, high specific surface area can facilitate the formation of small metallic nanoparticles with high metal surface exposed to reactants. In the current work, the catalysts with lower metallic nanoparticle size (Pd-Cu/ENS350 and Pd-Cu/AC) showed the highest activity, but Pd-Cu/ENS250, with the largest nanoparticle size (8.7 nm), showed an activity close to that observed for Pd-Cu/AC. Moreover, the catalysts supported on CNF, rGO and G with intermediate nanoparticle size (3.8-6.5 nm), showed the lowest activity. Thus, no direct relationship between metallic particle size and activity was found. The effect of the nanoparticle size on catalytic activity was investigated by different authors in literature, but no general agreement was found. For instance, Shafqat et al. [21] assessed the influence of Pt size of monometallic Pt/silica catalysts in catalytic NO₃⁻ reduction, showing that the largest particles (8 nm) in their range of study (2-8 nm) were related to higher activity. Papa et al. [22] studied NO₃⁻ reduction with Pd-Cu catalysts of different nanoparticle size supported onto titania and alumina and found that those with smaller nanoparticle size (4.1 and 6.2 nm) showed higher NO₃⁻ conversion compared to larger ones (13 and 15 nm). Therefore, no conclusive results have been observed in literature regarding the influence of specific surface area and mean

nanoparticle size in catalytic activity, evidencing that additional features of the catalytic system can have a relevant role.

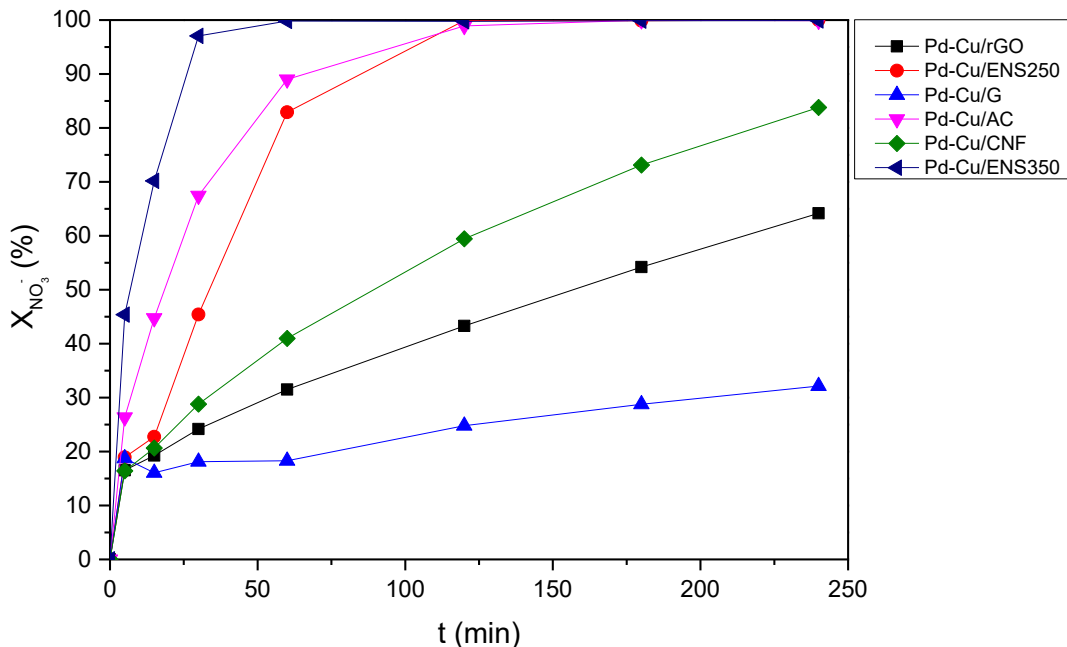


Figure 4. NO_3^- conversion vs reaction time for the catalysts tested ($[\text{NO}_3^-]_0 = 100 \text{ mg/L}$, H_2 flow: 50 N mL/min, CO_2 flow: 50 N mL/min, 0.4 g/L of catalyst)

Figure 5a depicts the selectivity to NH_4^+ vs NO_3^- conversion for all the catalysts tested. The Pd-Cu/rGO catalyst showed a higher ability to produce NH_4^+ at any NO_3^- conversion above 20 %. At ca. 65 % of NO_3^- conversion, this catalyst showed a selectivity to NH_4^+ of 50%, whereas the catalyst supported on AC showed 35 %. Pd-Cu/CNF and Pd-Cu/ENS350 catalysts exhibited equivalent selectivity to NH_4^+ (ca. 6 %), whereas Pd-Cu/ENS250 showed the lowest value: around 1 %. The activity of Pd-Cu/G was very low, reaching NO_3^- conversion values lower than 35 % and making difficult the comparison to other catalysts.

With the aim of further exploring the behavior of those catalysts supported on rGO, CNF, G at high NO_3^- conversion, catalytic runs with lower initial NO_3^- concentration (20 mg /

L) were performed (Figure 5b). NO_3^- conversion increased up to 85 % in the case of Pd-Cu/rGO catalyst and to 100 % in the case of Pd-Cu/G and Pd-Cu/CNF. When compared at 80-85 % of NO_3^- conversion, the selectivity to NH_4^+ was 50-55 %, 21 % and 5-7 % for the Pd-Cu/rGO, Pd-Cu/G and Pd-Cu/CNF catalysts, respectively. The selectivity to NH_4^+ is higher for the reactions at high nitrate concentration (Figure 5a), showing that competence among species for the active sites, probably from early stages of the experiment, can decrease the accumulation of intermediate N species. This effect can be observed from the lower increase of NH_4^+ at nearly complete NO_3^- conversion.

From the results in Figures 5a and 5b, it has to be noted that the three catalysts yielding lower selectivity to NH_4^+ are characterized by good conductivity of the support, and that two of them show the largest nanoparticle size (Pd-Cu/ENS250 and Pd/CNF). In this sense, Yoshinaga et al. [20] reported that selectivity to N_2 increased with Pd crystallite size since the Pd edges and corners have higher hydrogenation ability. They also indicated that the deposition of Cu atoms on Pd edges and corners could also avoid the formation of NH_4^+ , favoring the selectivity to N_2 . However, in the current work, one of the catalysts yielding low selectivity to NH_4^+ had also the smallest nanoparticle size (Pd-Cu/ENS350). Interestingly, ENS350 was one of the most conductive supports tested in this work. In the case of Pd-Cu/CNF catalyst, it has a highly conductive support and relatively large nanoparticle size among the tested. This catalyst only showed a significant increase of the selectivity to NH_4^+ at close to 100 % conversion, which can be related to the high H/N ratio occurring once the NO_3^- concentrations on the catalyst surface is very low, and uptaken intermediate N species evolve to NH_4^+ [23]. rGO is the less conductive of the supports tested and Pd-Cu/rGO catalyst showed the highest NH_4^+ formation. Li et al. [24] reported that charge transfer from metal to support can change the adsorption and activation of intermediate species on Ru/ TiO_2 catalysts in CO_2 hydrogenation, probably

due to the different extent of H₂ spill-over, affecting the selectivity. They observed a high activation of intermediate species in the cases where less charge transfer occurred, thus leading to deep hydrogenation to CH₄. On the contrary, higher charge transfer led to a weakening in adsorption and activation of the intermediates, favoring selectivity to CO. Rao et al. [25] reported that charge transfer not only takes place between noble metal and metal oxides supports, as they evidenced the influence on the selectivity of charge transfer between Pd and CNT support in the hydrogenation of cinnamaldehyde. Hydrogenation of C=O or C=C was effectively modulated by thermal treatment of the support at 1000 °C provoking a higher charge transfer. They also proposed that a decrease in the work function of the graphenic layer of the CNT, caused by oxygen surface functionalities disappearance by annealing, could increase the difference between the work function of Pd and CNT, affecting to charge distribution. Therefore, conductive supports such as carbon blacks, CNF or G allow charge transfer between metal and carbon supports to occur, affecting to the adsorption and activation of the intermediate N species, and hindering the overreduction of intermediate N species to NH₄⁺.

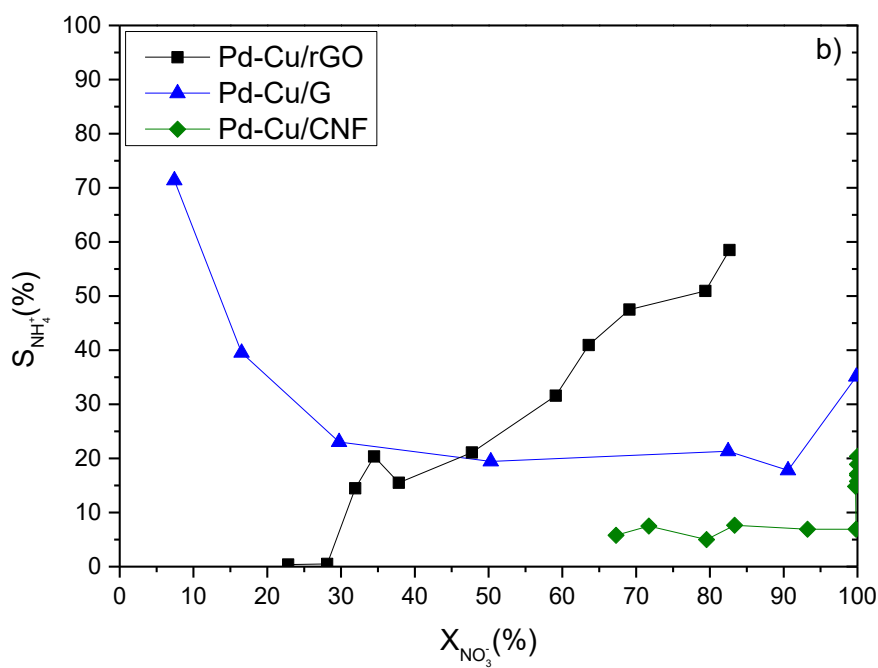
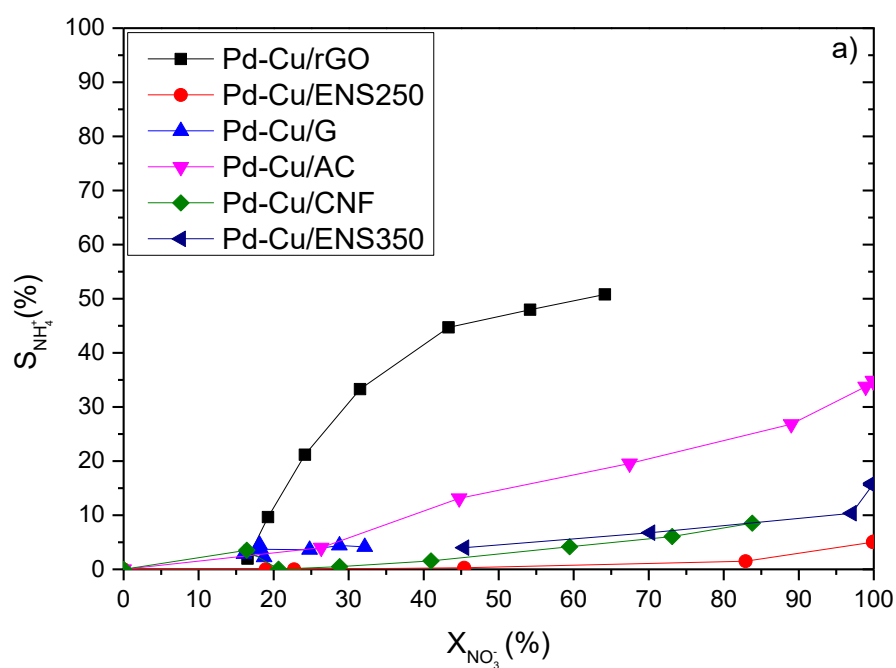


Figure 5. selectivity to NH_4^+ vs NO_3^- conversion a) $[\text{NO}_3^-]_0 = 100 \text{ mg/L}$ and b) $[\text{NO}_3^-]_0 = 20 \text{ mg/L}$ (H_2 flow: 50 N mL/min, CO_2 flow: 50 N mL/min, 0.4 g/L of catalyst)

3.3 Influence of H₂ availability on catalyst performance.

Figure 6 shows NO₃⁻ conversion vs time curves for Pd-Cu/rGO, Pd-Cu/CNF, Pd-Cu/ENS250 and Pd-Cu/ENS350 catalysts at different H₂ flow rates. In all the cases, the decrease in H₂ flow led to a decrease in NO₃⁻ conversion, being this effect especially pronounced for those catalysts with higher activity, i.e. Pd-Cu/ENS250 and Pd-Cu/ENS350. H₂ was bubbled into the reaction system together with CO₂, therefore a lower H₂ flow can be assumed to lead to lower H₂ partial pressure in the system, and in turn lower amount of H₂ available in the aqueous media for reduction reaction. In this conditions H₂ may become the limiting reagent because of its lower concentration and lower mass transfer rate.

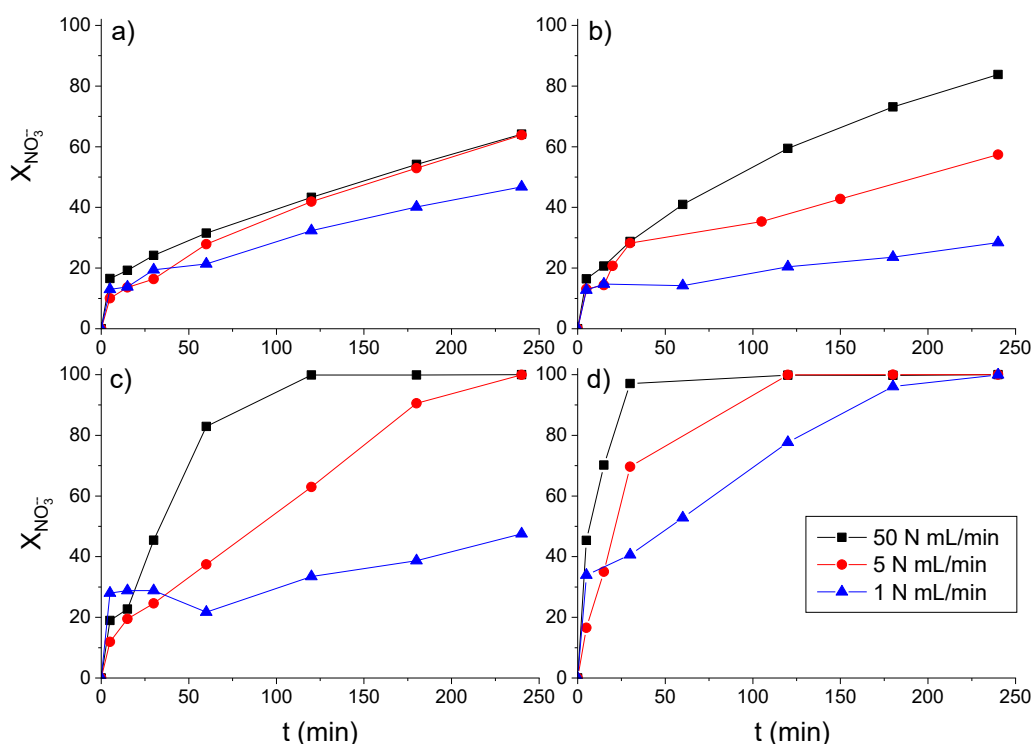


Figure 6. NO₃⁻ conversion upon reaction time for a) Pd-Cu/rGO; b) Pd-Cu/CNF; c) Pd-Cu/ENS250 and d) Pd-Cu/ENS350 at different H₂ flow ([NO₃⁻]₀ = 100 mg /L, CO₂ flow: 50 N mL/min, 0.4 g/L of catalyst)

Figure 7 shows the selectivity to NH_4^+ vs NO_3^- conversion curves for Pd-Cu/rGO, Pd-Cu/CNF, Pd-Cu/ENS250 and Pd-Cu/ENS350 catalysts at different H_2 flow rates. The decreasing H_2 flow resulted in a lower selectivity to NH_4^+ that can be more clearly observed in the case of Pd-Cu/rGO and Pd-Cu/ENS250 catalysts. This can be related to a lower H_2 availability that limits the H/N ratio and overreduction of intermediate N species at catalytic sites. In the case of Pd-Cu/CNF and Pd-Cu/ENS250 the differences in activity of these catalysts at different H_2 flows, hinders comparison at the 3 different flows tested. The release of NH_4^+ for nearly complete NO_3^- conversion was not suppressed, but in general lower release was observed in the test were the availability of H_2 was lower.

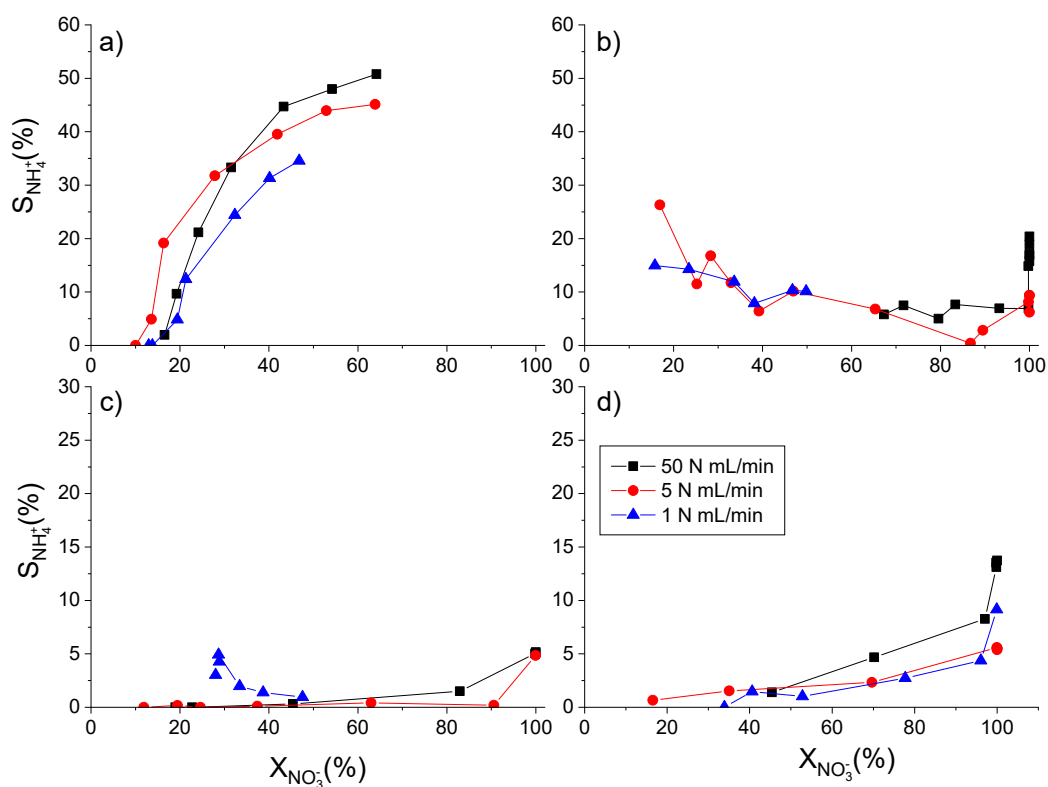


Figure 7. Selectivity to NH_4^+ vs NO_3^- conversion for a) Pd-Cu/rGO; b) Pd-Cu/NFC; c) Pd-Cu/ENS250 and d) Pd-Cu/ENS350 at different H_2 flows. $[\text{NO}_3^-]_0 = 100 \text{ mg/L}$

3.3.1 Mass transfer regime study

Table 3 shows the calculated Ca_{G-L} , Ca_{L-S} , $(\Phi_s)_{H_2}$, and $(\Phi_s)_{NO_3^-}$ values for the reactions carried out with Pd-Cu/rGO, Pd-Cu/CNF, Pd-Cu/ENS250, and Pd-Cu/ENS350 catalysts at different H_2 flows. According to Ca_{G-L} values, mass transfer limitations cannot be ruled out for any of the catalysts when tested at the lowest H_2 flow (1 N mL/min). Likewise, mass transfer cannot be ruled either for Pd-Cu/ENS250 and Pd-Cu/ENS350 catalysts at a H_2 flow of 5 N mL/min. It must be noted that some authors used a more restrictive criterion ($Ca < 0.05$) to discard mass transfer limitations [26, 27]. According to this last, mass transfer limitations could not be ruled out at ≤ 5 N mL/min of H_2 flow for any of the catalysts. Moreover, the Ca_{G-L} values for Pd-Cu/ENS250 and Pd-Cu/ENS350 catalysts were under but quite close to the limit (0.034-0.041) at 50 N mL/min flow. These results are in good agreement with the trends observed for the activity (Fig. 6) and the selectivity to NH_4^+ (Fig. 7), where lower values of activity and selectivity can be observed for the experiments where lower H_2 flows were used. The change in selectivity was evident even for Pd-Cu/rGO, whose activity did not decay so drastically with decreasing H_2 flow. In the case of Ca_{L-S} and Weisz-Prater modules, values were low enough to rule out mass transfer or intraparticle diffusion limitations. Therefore, changes in the behavior of the catalysts can be ascribed to external mass transfer.

Table 3. Ca_{G-L} , Ca_{L-S} , $(\Phi_s)_{H_2}$, and $(\Phi_s)_{NO_3^-}$ at different H_2 flows for Pd-Cu/rGO, Pd-Cu/CNF, Pd-Cu/ENS250, and Pd-Cu/ENS350 catalysts

Catalyst	H_2 flow (N mL/min)	Ca_{G-L} ($\cdot 10^{-2}$)	$Ca_{L-S}H_2$ ($\cdot 10^{-6}$)	$Ca_{L-S}NO_3^-$ ($\cdot 10^{-7}$)	$(\Phi_s)_{H_2}$ ($\cdot 10^{-4}$)	$(\Phi_s)_{NO_3^-}$ ($\cdot 10^{-4}$)
Pd-Cu/rGO	50	1.0	0.3	0.9	2.0	0.7
	5	9.1	1.3	0.7	9.1	0.6
	1	43	3.8	0.5	28	0.4
Pd-Cu/CNF	50	1.5	0.4	5.9	2.7	4.9
	5	5.1	0.7	2.0	5.1	1.7
	1	9.5	0.8	0.5	6.1	0.4
Pd-Cu/ENS250	50	3.4	0.9	2.8	6.5	2.3
	5	13	1.8	1.0	13	0.8
	1	44	3.9	0.5	29	0.4
Pd-Cu/ENS350	50	4.1	1.1	3.4	7.8	2.8
	5	45	6.2	3.5	45	2.9
	1	154	14	1.7	99	1.4

4. Conclusions

The use of carbon materials with different structure as catalyst supports allows bimetallic Pd-Cu catalysts to achieve different behavior in terms of NO_3^- conversion and selectivity to NH_4^+ . Catalysts supported on carbon materials with high specific surface area showed nearly complete NO_3^- conversion. This behavior can be linked to better dispersion of the metallic phase, but catalysts supported on ENS250 carbon black showed relatively high activity in spite of their relatively low specific surface and large size of metallic nanoparticles, suggesting that conductivity of the support also could contribute to NO_3^- conversion. Catalysts with supports of relatively high or moderate conductivity, showed lower selectivity to NH_4^+ , especially in the case of carbon blacks (ENS250 and ENS350) and CNF, which can be ascribed to charge transfer from metal to support. When H_2 flow was reduced in the catalytic runs, NO_3^- conversion and selectivity to NH_4^+ also diminished, suggesting that mass transfer limitation can occur at low H_2 flows. The analysis of the parameters describing mass transfer revealed external gas-liquid mass transfer limitations for H_2 . Ca_{G-L} values above 0.05 (limiting value) were achieved when

H₂ flow of 1 and 5 N mL/min were used, which in turn resulted in a decay in NO₃⁻ conversion and selectivity to NH₄⁺. The results obtained indicate that approaches based on the control of mass transfer can be useful to control selectivity to NH₄⁺, and combination with catalysts properties such as conductivity of the supports makes possible additional control.

Acknowledgements

The authors greatly appreciate the support from Spanish Agencia Estatal de Investigación (AEI, RTI2018-098431-BI00). Dydia Tanisha González thanks the Regional Government of Madrid a research grant (PEJ-2020-AI/AMB-17551) and Adrián Marí thanks the Spanish AEI a research grant (PRE-2019-088601).

References

- [1] K. Vorlop, T. Tacke, Erste Schritte auf dem Weg zur edelmetallkatalysierten Nitrat- und Nitrit-Entfernung aus Trinkwasser, Chem. Ing. Tech. 61 (1989) 836-837. <https://doi.org/10.1002/cite.330611023>
- [2] J. Martínez, A. Ortiz, I. Ortiz, State-of-the-art and perspectives of the catalytic and electrocatalytic reduction of aqueous nitrates, Appl. Catal. B: Env. 207 (2017) 42-59. <https://doi.org/10.1016/j.apcatb.2017.02.016>.
- [3]. Council Directive 98/83/EC of 3 November 1998 on the quality of water intended for human consumption, ANNEX I: PARAMETERS AND PARAMETRIC VALUES, PART B: Chemical parameters. EUR-Lex. Retrieved 11th May 2021. <https://eur-lex.europa.eu/legal-content/EN/TXT/HTML/?uri=CELEX:31998L0083&from=EN>.
- [4] N. Barrabés, J. Sá, Catalytic nitrate removal from water, past, present and future perspectives, Appl. Catal. B: Env. 104 (2011) 1-5. <https://doi.org/10.1016/j.apcatb.2011.03.011>
- [5] O.S.G.P. Soares, J.J.M. Órfão, M.F.R. Pereira, Nitrate reduction in water catalysed by Pd-Cu on different supports, Desalination 279 (2011) 367-374. <https://doi.org/10.1016/j.desal.2011.06.037>.

- 451 [6] A.S. Santos, J. Restivo, C.A. Orge, M.F. Pereira, O.S. Soares, Nitrate Catalytic
452 Reduction over Bimetallic Catalysts: Catalyst Optimization, *C* 6(4) (2020) 78.
453 <https://doi.org/10.3390/c6040078>.
- 454 [7] R.S. Postma, R. Brunet Espinosa, L. Lefferts, Competitive Adsorption of Nitrite and
455 Hydrogen on Palladium during Nitrite Hydrogenation, *ChemCatChem* 10 (2018) 3770-
456 3776. <https://doi.org/10.1002/cctc.201800523>.
- 457 [8] J.A. Baeza, F. García-Missana, A.S. Oliveira, L. Calvo, M.A. Gilarranz, Influence of
458 H₂ availability in the catalytic reduction of nitrates in fixed bed reactors, *Chem. Eng.*
459 *Sci.*, (2021) 116887. <https://doi.org/10.1016/j.ces.2021.116887>
- 460 [9] H. Yagi, F. Yoshida, Gas Absorption by Newtonian and Non-Newtonian Fluids in
461 Sparged Agitated Vessels, *Ind. Eng. Chem. Proc. Des. Dev.* 14 (1975) 488-493.
462 <https://doi.org/10.1021/i260056a024>
- 463 [10] K. Miyabe, R. Isogai, Estimation of molecular diffusivity in liquid phase systems
464 by the Wilke–Chang equation, *J. Chromatogr., A* 1218 (2011) 6639-6645.
465 <https://doi.org/10.1016/j.chroma.2011.07.018>
- 466 [11] W. Ranz, W. Marshall, Evaporation from drops, *Chem. Eng. Prog.* 48 (1952) 141-
467 146.
- 468 [12] H.H. Lee, *Heterogeneous reactor design*; Sponsor Org., Butterworth Publishers,
469 Stoneham, MA, United States, 1984.
- 470 [13] B. P. Chaplin, E. Roundy, K. A. Guy, J. R. Shapley, C. J. Werth. Effects of Natural
471 Water Ions and Humic Acid on Catalytic Nitrate Reduction Kinetics Using an Alumina
472 Supported Pd–Cu Catalyst. *Environ. Sci. Technol.* 2006, 40, 9, 3075.
473 <https://doi.org/10.1021/es0525298>
474
- 475 [14] F.A. Marchesini, G. Mendow, N.P. Picard, F.M. Zoppas, V.S. Aghemo, L.B.
476 Gutierrez, C.A. Querini, E E. Miró. PdIn Catalysts in a Continuous Fixed Bed Reactor
477 for the Nitrate Removal from Groundwater *Int. J. Chem. React. Eng.* 2019, 20180126.
478 <https://doi.org/10.1515/ijcre-2018-0126>
- 479 [15] P. Granger, S.Tronc  a, J.P. Dacquin, M. Trentesaux, O. Gardoll, N.Nuns,
480 V.I.Parvulescu. Peculiar kinetic properties of Cu-doped Pd/Ce_xZr_{1-x}O₂ in water
481 denitrification: Impact of Pd-Cu interaction vs structural properties of Ce_xZr_{1-x}O₂. *Appl.*
482 *Catal. B: Env.* 2019, 253, 391. <https://doi.org/10.1016/j.apcatb.2019.04.010>
- 483 [16] J. B. Butt, *Reaction Kinetics and Reactor Design*, second edition ed., CRC Press,
484 New York, 2000.
- 485 [17] X. Jiao, Y. Qiu, L. Zhang, X. Zhang, Comparison of the characteristic properties of
486 reduced graphene oxides synthesized from natural graphites with different
487 graphitization degrees, *RSC Adv.* 7 (2017) 52337-52344.
488 <https://doi.org/10.1039/C7RA10809E>

- 489 [18] T. Qiu, J. Yang, X. Bai, Y. Wang, The preparation of synthetic graphite materials
490 with hierarchical pores from lignite by one-step impregnation and their characterization
491 as dye absorbents, *RSC Adv.* 9 (2019) 12737-12746.
492 <https://doi.org/10.1039/C9RA00343F>
- 493 [19] M. Al Bahri, L. Calvo, M.A. Gilarranz, J.J. Rodriguez, F. Epron, Activated carbon
494 supported metal catalysts for reduction of nitrate in water with high selectivity towards
495 N₂, *Appl. Catal. B: Env.* 138-139 (2013) 141-148.
496 <https://doi.org/10.1016/j.apcatb.2013.02.048>
- 497 [20] Y. Yoshinaga, T. Akita, I. Mikami, T. Okuhara, Hydrogenation of Nitrate in Water
498 to Nitrogen over Pd–Cu Supported on Active Carbon, *J. Catal.* 207 (2002) 37-45.
499 <https://doi.org/10.1006/jcat.2002.3529>.
- 500 [21] K. Shafqat, S. Pitkäaho, M. Tiainen, L. Matějová, R.L. Keiski, Effect of
501 Nanoparticle Size in Pt/SiO₂ Catalyzed Nitrate Reduction in Liquid Phase,
502 *Nanomaterials* 11 (2021) <https://doi.org/10.3390/nano11010195>.
- 503 [22] F. Papa, I. Balint, C. Negrila, E. Olaru, I. Zgura, C. Bradu, Supported Pd–Cu
504 Nanoparticles for Water Phase Reduction of Nitrates. Influence of the Support and of
505 the pH Conditions, *Ind. Eng. Chem. Res.* 53 (2014) 19094-19103.
506 <https://doi.org/10.1021/ie503070f>.
- 507 [23] S.D. Ebbesen, B.L. Mojet, L. Lefferts, In situ ATR-IR study of nitrite
508 hydrogenation over Pd/Al₂O₃, *J. Catal.* 256 (2008) 15-23.
509 <https://doi.org/10.1016/j.jcat.2008.02.013>
- 510 [24] X. Li, J. Lin, L. Li, Y. Huang, X. Pan, S.E. Collins, Y. Ren, Y. Su, L. Kang, X.
511 Liu, Y. Zhou, H. Wang, A. Wang, B. Qiao, X. Wang, T. Zhang, Controlling CO₂
512 Hydrogenation Selectivity by Metal-Supported Electron Transfer, *Angew. Chem. Int.*
513 *Ed.* 59 (2020) 19983-19989. <https://doi.org/10.1002/anie.202003847>
- 514 [25] R.G. Rao, R. Blume, T.W. Hansen, E. Fuentes, K. Dreyer, S. Moldovan, O. Ersen,
515 D.D. Hibbitts, Y.J. Chabal, R. Schlögl, J. Tessonier, Interfacial charge distributions in
516 carbon-supported palladium catalysts, *Nat. Commun.* 8 (2017) 340.
517 <https://doi.org/10.1038/s41467-017-00421-x>
- 518 [26] L. Ronchin, L. Toniolo, Selective hydrogenation of benzene to cyclohexene using a
519 suspended Ru catalyst in a mechanically agitated tetraphase reactor, *Catal. Today* 48
520 (1999) 255-264. [https://doi.org/10.1016/S0920-5861\(98\)00380-0](https://doi.org/10.1016/S0920-5861(98)00380-0)
- 521 [27] J. Dam, A. Ramanathan, K. Djanashvili, F. Kapteijn, U. Hanefeld, Synthesis,
522 characterization and performance of bifunctional catalysts for the synthesis of menthol
523 from citronellal, *RSC Adv.* 7 (2017) 12041-12053.
524 <https://doi.org/10.1039/C6RA25931F>

Enhancement of activity and selectivity to nitrogen in catalytic nitrate reduction by use of conductive carbon catalytic supports and control of hydrogen mass transfer regime

D.T. González, A. Marí, J.A. Baeza, L. Calvo*, M.A. Gilarranz

Departamento de Ingeniería Química, C/Francisco Tomás y Valiente 7, Universidad Autónoma de Madrid, 28049 Madrid, Spain

*corresponding author e-mail: luisa.calvo@uam.es

Abstract

Carbon materials with different structural properties (activated carbon, carbon nanofibers, reduced graphene oxide, graphite, and carbon black) were used as supports of Pd-Cu (5 wt. %) catalysts for the catalytic reduction of NO_3^- in batch reactors. In general, those catalyst with smaller metal nanoparticles and carbon supports with higher specific surface area were more active, although remarkable activity was also observed for catalysts with relatively large nanoparticles and conductive supports. Conductivity of carbon supports also contributed to a lower selectivity to NH_4^+ , which can be ascribed to higher charge transfer between metal and support reducing activation of intermediate species. The decrease of H_2 feed into the reaction system resulted in external (gas-liquid) mass transfer constrains, as evidenced by the parameters describing control regime, and led to diminished NH_4^+ selectivity, particularly in the case of catalysts with conductive supports. Approaches combining control of mass transfer regime and conductive carbon catalytic supports can be useful to enhance selectivity to N_2 , which is a major challenge in catalytic NO_3^- reduction.

Keywords

NO_3^- reduction, carbon, conductive supports, Pd-Cu catalysts, mass transfer limitations

1. Introduction

Catalytic reduction of NO_3^- was firstly reported by Vorlop et al. [1], since then, it has attracted much attention as an interesting alternative for drinking water treatment. The process consists in the catalytic reduction of NO_3^- using H_2 (or a source of H_2) at temperatures and pressures near ambient ones. The relatively low operation costs and the absence of post-treatment are among the main advantages of this process compared with traditional physicochemical and biological treatments. The most accepted mechanism for the catalytic reduction of NO_3^- proposes firstly NO_3^- reduction to NO_2^- , and secondly NO_2^- reduction to N_2 or NH_4^+ , through N-containing intermediate species adsorbed on catalysts surface [2]. EU regulation establishes 50, 0.1 and 0.5 mg/L as limits in drinking water for NO_3^- , NO_2^- and NH_4^+ , respectively [3].

The proper control of the selectivity to undesired products (i.e. NO_2^- , NH_4^+) is still a challenge. Several variables influencing the reduction mechanism and the selectivity to NH_4^+ such as the type of reactor, pH, catalysts, and operating conditions, among others, are known [2, 4]. Different metallic phases and supports have been studied to better understand catalyst influence on selectivity. Regarding the metallic phase, Rh, Pt and Pd are widely used [4], being the latter one of the most used noble metals due to its good ability to reduce NO_3^- . A second metal is commonly used as it promotes in the first step the reduction from NO_3^- to NO_2^- through a redox cycle involving Pd and H_2 . Different promoter metals such as Sn, In or Cu are among the most used. [2]

A great variety of catalyst supports including zeolites, titania, ceria, alumina, clays and carbon materials, especially activated carbon, have been used in catalytic NO_3^- reduction [5]. Carbon materials are versatile and present noticeable features such as inertness, hydrothermal stability, and facility to recover metallic phase, among others [6]. Moreover, their physical and chemical composition can be tailored through different

methods. Carbon materials are found in a great number of different structures leading to different properties, which makes them suitable candidates to study the role of supports in catalytic activity and selectivity. Activated carbon has been widely used as carbon support in catalytic NO_3^- reduction due to their large surface area, however, some authors [5] have reported that surface area not always has a significant influence on activity. Carbon supports with more ordered structure, such as graphite (G), carbon nanofibers (CNF) or carbon blacks, have been less studied probably due to their lower surface area. Nevertheless, these supports with a more ordered structure could facilitate charge delocalization and transfer, and could have an impact on activity and/or selectivity given the redox nature of the reactions involved.

Another crucial variable influencing activity and selectivity is the availability of reducing agent at catalytic centers. A high concentration of H_2 in the reactor system can lead to an increase in NO_3^- and NO_2^- conversion rate, but also an increase in selectivity to NH_4^+ . High H:N ratios at active sites lead to overreduction of the N-containing intermediate species adsorbed, since N-H bonds formation is favored compared to N-N bonds [7]. In a recent work [8], we have reported on the relevance of establishing operating conditions leading to mass transfer limitations for H_2 in fixed bed reactors as an approach to control selectivity to NH_4^+ .

In the present work, carbon materials with different structural ordering have been studied as supports for bimetallic Pd-Cu metallic phase and in batch NO_3^- reduction. Moreover, the influence of H_2 availability in the reaction system was studied, and the parameters describing H_2 transfer in the system and their links with catalyst performance were assessed.

2. Experimental

2.1 Materials

PdCl₂ (> 99.9 %), CuCl₂·2H₂O (> 99.9 %), graphite (G), graphitized carbon nanofibers (CNF) and 2,6-Pyridinedicarboxylic acid (> 99.5 %) were provided by Sigma-Aldrich. NaNO₃ (99 %), NaNO₂ (98 %), NH₄Cl (99.5 %), Na₂CO₃ (99 %), NaHCO₃ (99.5 %) and HNO₃ (65 %) were supplied by Panreac. H₂ (> 99.999 %) and CO₂ (> 99.99 %) were supplied by Nippon gases. Reduced graphene oxide (rGO), activated carbon (AC), and carbon blacks ENSACO250G (ENS250) and ENSACO350G (ENS350) were purchased from Graphenea, Norit, and Timcal, respectively.

2.2. Catalysts preparation and characterization

Bimetallic catalysts (5 wt %) were prepared using Pd and Cu (2:1 wt %) as metallic phase and carbon materials as supports. The catalysts were prepared by successive wet impregnation. A PdCl₂ solution (4 mL) in 0.1 M HCl was mixed with 0.4 g of carbon support in a rotary-evaporator at 70°C, 200 rpm and 150 mbar until dryness. Then, this step was repeated with a CuCl₂·2H₂O (4 mL) solution. The catalysts were left overnight in an oven at 60 °C and, finally, calcined at 200 °C for 2 h and reduced at 200 °C under H₂ flow (25 N mL/min). The supports were characterized by N₂ adsorption-desorption at -196 °C (Tristar II, Micromeritics); XRD (X-pert PRO Theta/2Theta, Panalytical), where the stacking height (L_c) and crystallite size (L_a) parameters were calculated using Scherrer equation from (002) and (100) peaks.

Resistivity measurements were performed using a 4-point probe at different pressures (0-180 MPa). The catalysts were characterized by TEM (JEOL JEM 2100 with EDS, Oxford instruments). TEM micrographs were used to analyze nanoparticle mean diameter, standard deviation, and frequency histograms. At least 200 nanoparticles from different micrographs were counted for each catalyst.

2.3 Adsorption and catalytic runs

NO_3^- adsorption tests were carried out with all the carbon supports in a jacketed glass reactor at 30 °C and atmospheric pressure. 30-60 mg of support was placed into the reactor together with 150 mL of a 100 mg/L NO_3^- solution under stirring (800 rpm) for 4 h. Catalytic runs were also carried out at 30 °C and atmospheric pressure using the same experimental setup described for the adsorption tests. A typical run started with 140 mL of water mixed with a known amount of catalysts (30-60 mg) and subjected to vigorous stirring (800 rpm) under H_2 (50 N mL/min) and CO_2 (50 N mL/min) flows for 30 min. Then a concentrated solution of NO_3^- (10 mL) was added to reach the desired initial concentration (20-100 mg/L) at $t = 0$. The liquid samples (1 mL) were collected and filtered (PTFE filter, pore size 0.22 μm) before their analysis. Liquid chromatography (Metrohm 882 Compact IC plus anion and cation) with a Metrosep C4 column using a 1.7 mM HNO_3^- + 0.7 mM 2,6-Pyridinedicarboxylic acid eluent (0.9 mL/min) was used for cation separation. A Metrosep A Supp 5 column and 3.2 mM Na_2CO_3 + 1 mM NaHCO_3 eluent (0.7 mL/min) was used for anion separation. NO_3^- conversion and selectivity to NO_2^- and NH_4^+ were calculated according to Eqs. 3, 4 and 5, respectively, where $n_{A, t=0}$ is the initial of amount of compound A (mol) and $n_{A, t}$ is the amount of compound A (mol) at time t (min).

$$X_{\text{NO}_3^-}(\%) = \frac{n_{\text{NO}_3^-, t=0} - n_{\text{NO}_3^-, t}}{n_{\text{NO}_3^-, t=0}} \cdot 100 \quad (3)$$

$$S_{\text{NO}_2^-}(\%) = \frac{n_{\text{NO}_2^-, t}}{n_{\text{NO}_3^-, t=0} - n_{\text{NO}_3^-, t}} \cdot 100 \quad (4)$$

$$S_{\text{NH}_4^+}(\%) = \frac{n_{\text{NH}_4^+, t}}{n_{\text{NO}_3^-, t=0} - n_{\text{NO}_3^-, t}} \cdot 100 \quad (5)$$

2.4 Mass transfer regime study

With the aim of assessing the behavior of the catalysts at different H₂ flow conditions, a mass transfer regime study was carried out. The external mass transfer was assessed through the calculation of the Carberry number for the gas-liquid (Ca_{G-L}) and liquid-solid (Ca_{L-S}) mass transfer, respectively, according to Eqs. 6 and 7.

$$Ca_{G-L} = \frac{R(i)_{obs}}{K_L a_v \cdot C_i^*} \quad (6)$$

$$Ca_{L-S} = \frac{R(i)_{obs}}{K_S a_p \cdot C_i^*} \quad (7)$$

where $R(i)_{obs}$ (mmol/L·s) corresponds to the observed reaction rate for H₂ transfer and H₂ and NO₃⁻ for Ca_{G-L} and Ca_{L-S} , respectively. $R(NO_3^-)_{obs}$ could not be calculated strictly as initial rate because for some catalysts the effect of nitrate adsorption was significant at short reaction times. Reaction rate was calculated up to ca. 50% conversion as long as a linear trend was maintained. The denominator in both Eqs. 6 and 7 corresponds to the maximum external mass transfer rate ($R(i)_{max}$), being $K_L a_v$ (s⁻¹) and $K_S a_p$ (s⁻¹) the gas-liquid and liquid-solid mass transfer coefficients and C_i^* the concentration of H₂ or NO₃⁻ (mmol/L) in the liquid phase or in the solid surface at equilibrium, assuming a maximum gradient of concentration across the boundary layer. In the case of H₂ the concentration was calculated by Henry's Law (Eq. 8). Mass transfer limitations can be discarded when Carberry number is lower than 0.1.

$$C_i = H \cdot P_i \quad (8)$$

where C_i corresponds to the H_2 concentration at equilibrium, H is the Henry's constant for the H_2/H_2O system and P_i is the partial pressure of H_2 in the medium. $K_L a_v$ was calculated from the dimensional correlation proposed by Yagi and Yoshida [9] (Eq. 9-13)

$$Sh = 0.06 \cdot Re^{1.5} \cdot Fr^{0.19} \cdot Sc^{0.5} \cdot \left(\frac{\mu_L \cdot u_g}{\sigma_L} \right)^{0.6} \cdot \left(\frac{d_I \cdot N}{u_g} \right)^{0.32} \quad (9)$$

$$Sh = \frac{K_L a_v \cdot d_I^2}{D_{mi}} \quad (10)$$

$$Re = \frac{d_I^2 \cdot N \cdot \rho_L}{\mu_L} \quad (11)$$

$$Fr = \frac{d_I \cdot N^2}{g} \quad (12)$$

$$Sc = \frac{\mu_L}{\rho_L \cdot D_{mi}} \quad (13)$$

where Sh , Re , Fr and Sc are the Sherwood, Reynolds, Froude, and Schmidt numbers, respectively. μ_L is the water viscosity (kg/m·s), u_g is the gas surface velocity (m/s), σ_L is the surface tension of water (kg/s), d_I is the magnetic stirrer diameter (m), ρ_L is the water density (kg/m³) and N is agitation velocity (s⁻¹), g is the gravity (m/s²) and D_{mi} is the molecular diffusivity calculated from Wilke-Chang equation [10] (Eq. 14)

$$D_{mi} = 7.4 \cdot 10^{-8} \cdot \frac{(\alpha \cdot M_w)^{0.5} \cdot T}{\mu_L \cdot V_i^{0.6}} \quad (14)$$

where α is the association coefficient (2.6 for water), M_w is the molecular mass of solvent (g/mol), T is the temperature (K), μ_L is solvent viscosity (g/cm·s) and V_i is the molar volume at the normal boiling point (cm³/mol)

$K_S a_p$ was estimated through Ranz and Marshall correlation [11] (Eq. 15) and Sherwood number (Eq. 16)

$$Sh = 2 + 0.6 \cdot Re^{1/2} \cdot Sc^{1/3} \quad (15)$$

$$Sh = \frac{k_s \cdot d_p}{D_{mi}} \quad (16)$$

where d_p corresponds to particle diameter and a_p can be expressed for spherical particles as $6/d_p$

Weisz-Prater criterion was used, as proposed by Lee [12] (Eq. 17) in order to analyze internal diffusion limitations. In first-order reactions using spherical catalysts, mass transfer limitations can be discarded when the Weisz-Prater module is lower than 1. First order kinetic constant was calculated from $\ln[\text{NO}_3^-]$ vs t plot. Different authors reported pseudo-first or first order kinetics in the catalytic reduction of nitrate using bimetallic Pd-based catalysts [13-15]

$$(\Phi_s)_i = \frac{R(i)_{obs} \cdot (d_p/6)^2}{C_i^* \cdot De_i} \quad (17)$$

Where De_i is the effective diffusivity of the compound i inside catalyst pores (cm^2/s). This was estimated, using Butt criteria, as 10 % of the molecular diffusivity in the liquid medium when tortuosity is unknown [16].

3. Results and discussion

3.1 Support and catalysts characterization

Table 1 shows the BET specific surface area (SSA_{BET}) and meso and micropore volume of the supports. Different SSA_{BET} from very low values (G, CNF) to relatively high (AC, ENS350) were obtained. Likewise, different pore volumes, from very low (G, CNF and ENS250) to relatively high (rGO, AC and ENS350) were observed.

Table 1. BET specific surface area, meso and micropore volume of the supports

Support	SSA_{BET} (m ² /g)	Mesopore volume (cm ³ /g)	Micropore volume (cm ³ /g)
G	2	0.04	0.003
CNF	4	0.06	0.005
rGO	86	0.59	0.12
AC	1210	0.38	0.53
ENS250	65	0.09	<0.001
ENS350	770	0.74	0.12

Figure 1 shows the X-ray diffractograms for the supports analyzed. All the patterns exhibited a diffraction peak at ca. 26° corresponding to the reflection plane of aromatic layers (002). This peak is related to the graphitization degree of carbon materials, being the orientation of the aromatic layers higher as the peak (002) gets narrower and more intense [17]. On the other hand, the samples showed another peak close to 42°, corresponding to the reflection plane (100) of aromatic layers. In the case of G, the plane (002) was related to the orientation of the aromatic layers in a 3-D arrangement, whereas the plane (100) was attributed to the degree of condensation of the aromatic carbon rings, thus, the peak (100) becomes narrower and higher as the size of the aromatic layer domains grows [18].

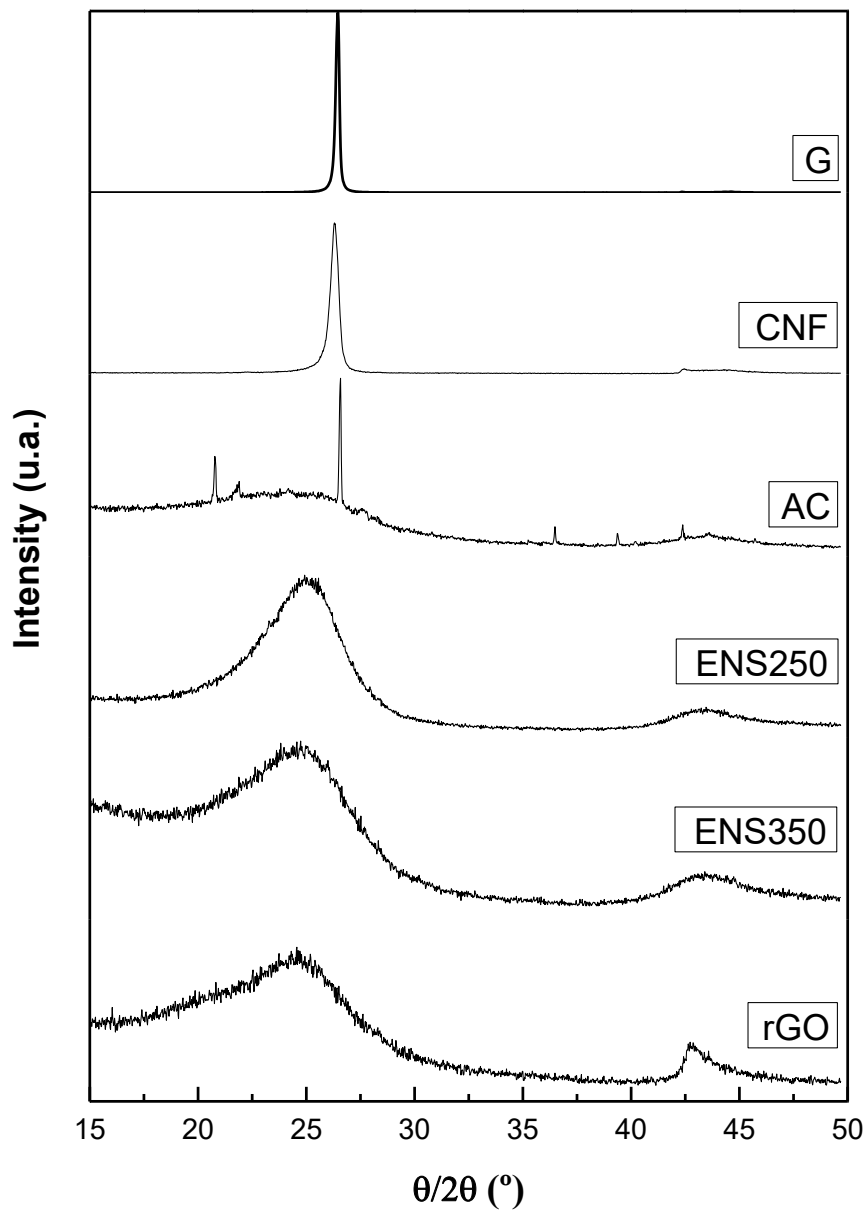


Figure 1. X-ray diffractograms for the carbon materials analyzed.

Table 2 represents L_c and L_a values for the different carbon materials. L_c values show that G and CNF are the supports with the highest stacking height, whereas the other supports are in a range of relatively low stacking height and small crystallite size. These results are good in agreement with Figure 1, where G and CNF show the sharpest (002) peaks among

the supports. Regarding to L_a , it was calculated only for the supports exhibiting a diffraction peak (001) clearly resolved. OGR, the most amorphous support, showed the highest value.

Table 2. L_c and L_a values for the different carbon materials studied.

Support	L_c (nm)	L_a (nm)
G	41.5	-
CNF	18.3	-
AC	1.4	-
ENS250	1.7	3.1
ENS350	0.6	2.5
rGO	0.7	8.2

Figure 2 represents the electrical resistivity vs pressure for the supports tested. It can be observed that increasing pressure from 0 to 37 MPa produced a decrease in resistivity due to sample compaction. In general, increasing pressure from 37 to 185 MPa did not lead to significant changes in resistivity, except for rGO, which can be ascribed to the very low density of the material (ca. 0.05 g/cm³), which results in ability for compaction. CNF and ENS350 are the most conductive supports and rGO is the less conductive, whereas AC, G and ENS250 showed an intermediate behavior. These measurements offered a reasonable approximation to the ability of the supports to transfer charge, but it must be noted that resistivity measurements were made on a carbon disk, and resistivity values may differ at real reaction conditions.

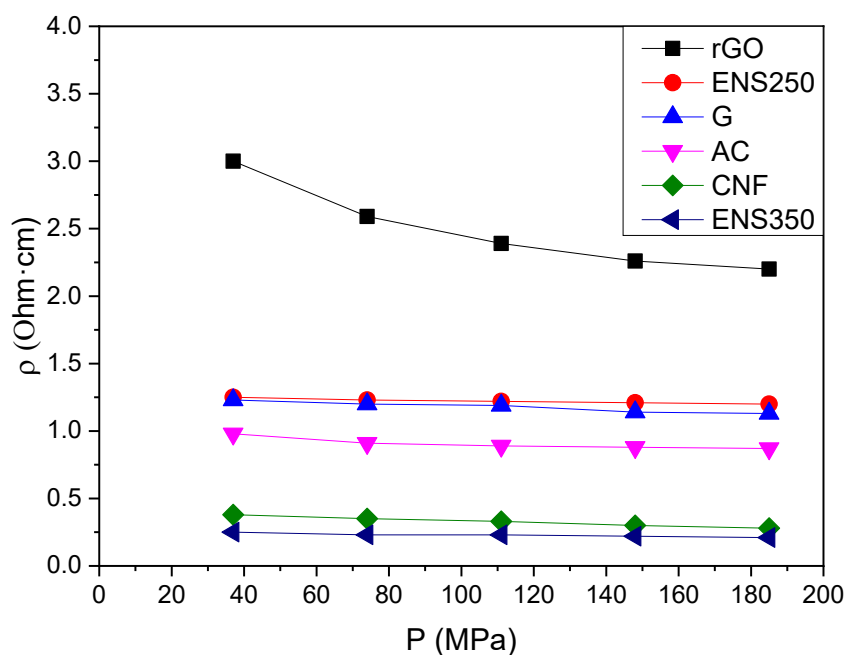
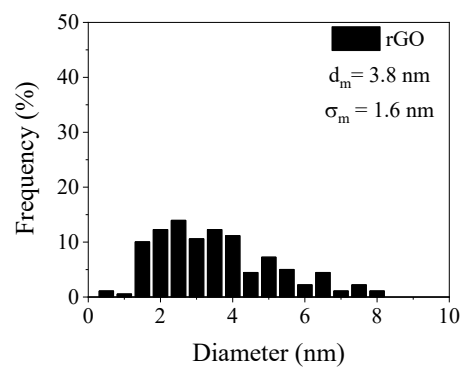
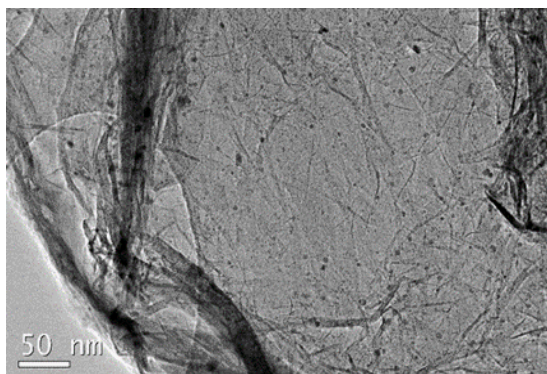
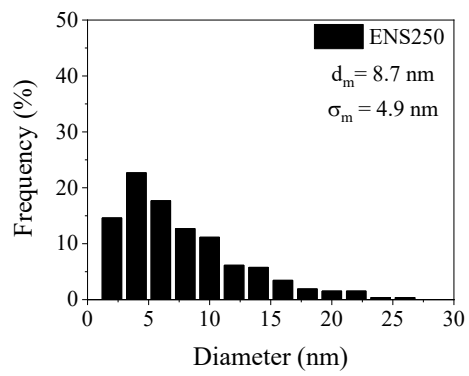
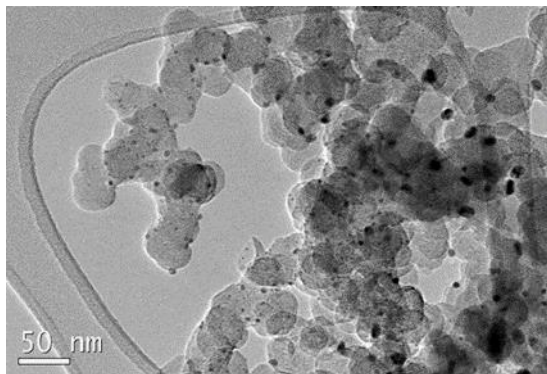
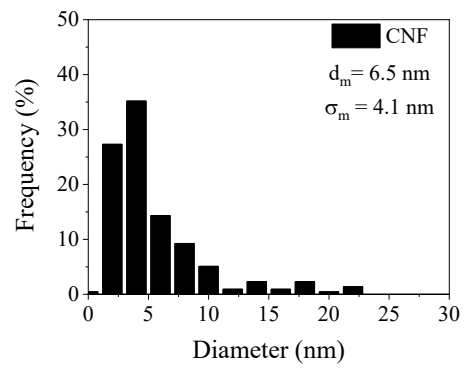
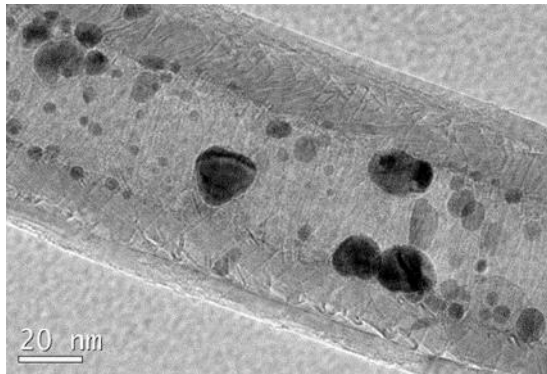
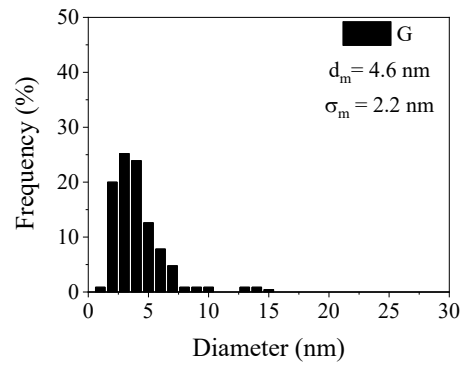
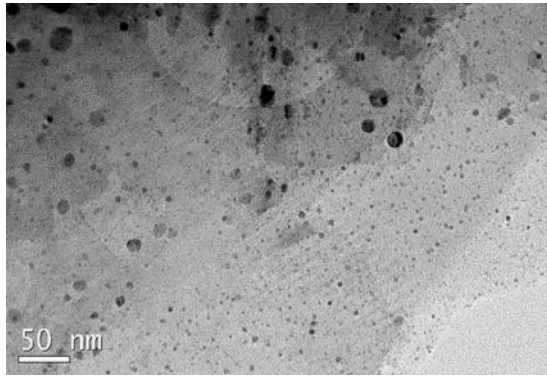


Figure 2. Resistivity vs Pressure curves for the supports tested.

Figure 3 shows representative TEM images showing dispersion of the metal phase, frequency histograms, nanoparticle mean size and standard deviation for all the catalyst prepared. Nanoparticle mean size and standard deviation were in a range from 1.4 to 8.7 nm and 0.4 to 4.9 nm, respectively. Pd-Cu/ENS350 and Pd-Cu/AC show both lower mean size and standard deviation, leading to well-dispersed small particles. ENS350 and AC supports present high specific surface area that facilitates metal dispersion. A higher amount of surface oxygen groups contributing to the formation of metal nuclei and limiting growth can also be expected in the case of AC [19]. On the other hand, Pd-Cu/CNF, and Pd-Cu/ENS250 show larger nanoparticle mean size and higher presence of larger particles (>10 nm) than the other catalysts.



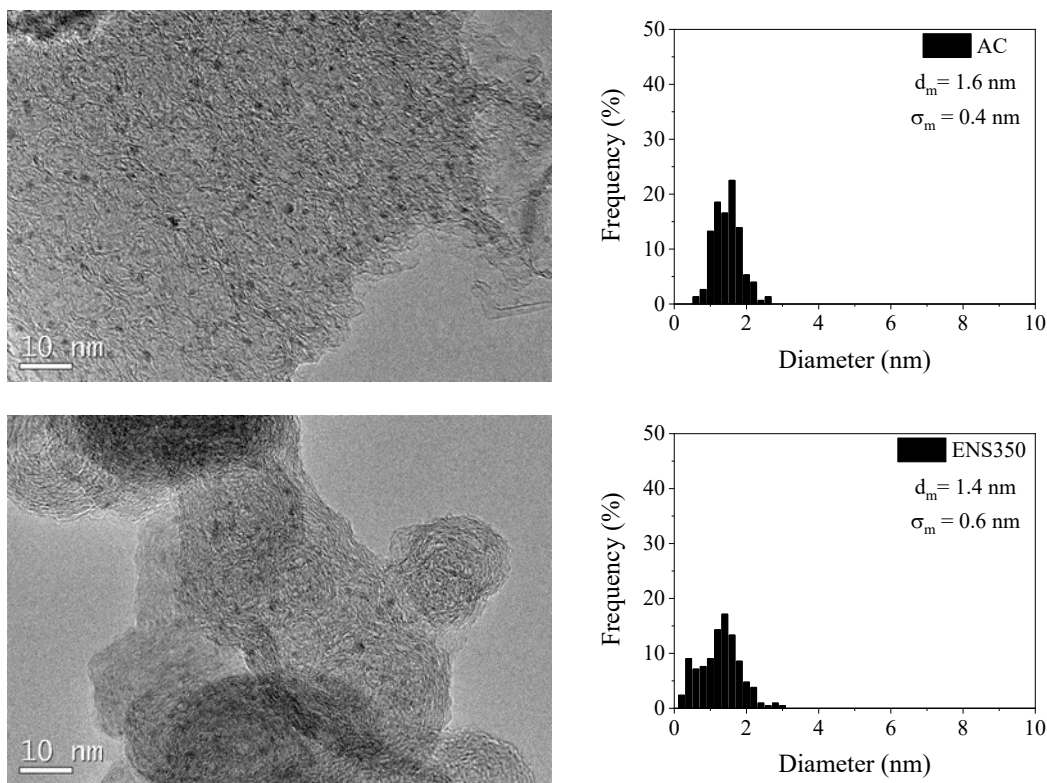


Figure 3. TEM images and nanoparticle size histograms for the catalysts prepared

3.2 Reaction tests

Previous to reaction tests, NO_3^- adsorption experiments using supports without metallic phase, both in the absence and the presence of H_2 and CO_2 , were carried out. The uptake of NO_3^- ranged between 1 and 16 %. Traces of NO_2^- and NH_4^+ were detected during the adsorption experiments when rGO, AC, ENS250 and ENS350 supports were tested, which indicates that supports barely contributed to NO_3^- conversion. No traces of reaction products were detected for NFC and G supports.

Figure 4 depicts NO_3^- conversion vs time curves for all the catalysts tested using a NO_3^- initial concentration of 100 mg/L. After 4 h, NO_3^- conversion was in a range from 32 to 100 %, being the catalysts supported on ENS350 and AC the most active ones. These supports presented the highest specific surface area (770-1210 m^2/g) among the set studied. Those catalysts with supports of low specific surface area, such as rGO, G or

CNF (2-86 m²/g), did not reach total conversion, except the one supported on ENS250 (65 m²/g), whose activity was slightly lower than that observed for Pd-Cu/AC. Yoshinaga et al. [20] studied the catalytic NO₃⁻ reduction using Pd-Cu supported on different materials such as alumina, zirconia, silica and activated carbon, reporting that high surface areas of the catalysts support led to high NO₃⁻ conversion. However, Soares et al. [5] found no significant effect of specific surface area on activity when they studied the performance of Pd-Cu bimetallic catalysts supported in several materials such as titania, AC, carbon nanotubes, manganese oxide, silica, ceria, etc.

As discussed above, high specific surface area can facilitate the formation of small metallic nanoparticles with high metal surface exposed to reactants. In the current work, the catalysts with lower metallic nanoparticle size (Pd-Cu/ENS350 and Pd-Cu/AC) showed the highest activity, but Pd-Cu/ENS250, with the largest nanoparticle size (8.7 nm), showed an activity close to that observed for Pd-Cu/AC. Moreover, the catalysts supported on CNF, rGO and G with intermediate nanoparticle size (3.8-6.5 nm), showed the lowest activity. Thus, no direct relationship between metallic particle size and activity was found. The effect of the nanoparticle size on catalytic activity was investigated by different authors in literature, but no general agreement was found. For instance, Shafqat et al. [21] assessed the influence of Pt size of monometallic Pt/silica catalysts in catalytic NO₃⁻ reduction, showing that the largest particles (8 nm) in their range of study (2-8 nm) were related to higher activity. Papa et al. [22] studied NO₃⁻ reduction with Pd-Cu catalysts of different nanoparticle size supported onto titania and alumina and found that those with smaller nanoparticle size (4.1 and 6.2 nm) showed higher NO₃⁻ conversion compared to larger ones (13 and 15 nm). Therefore, no conclusive results have been observed in literature regarding the influence of specific surface area and mean

nanoparticle size in catalytic activity, evidencing that additional features of the catalytic system can have a relevant role.

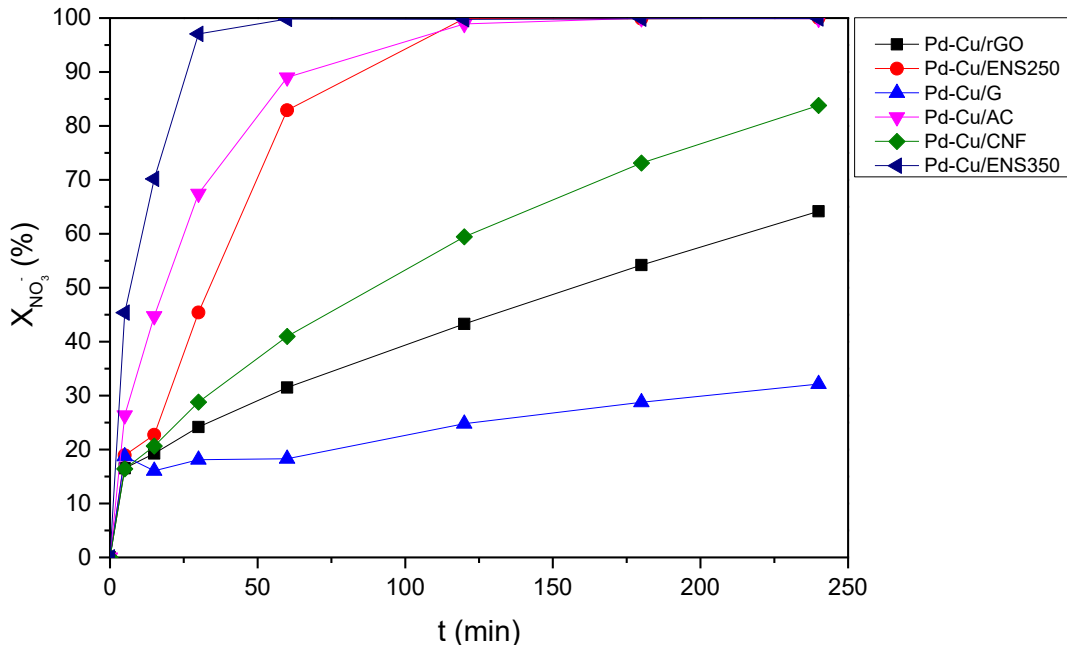


Figure 4. NO_3^- conversion vs reaction time for the catalysts tested ($[\text{NO}_3^-]_0 = 100 \text{ mg/L}$, H_2 flow: 50 N mL/min, CO_2 flow: 50 N mL/min, 0.4 g/L of catalyst)

Figure 5a depicts the selectivity to NH_4^+ vs NO_3^- conversion for all the catalysts tested. The Pd-Cu/rGO catalyst showed a higher ability to produce NH_4^+ at any NO_3^- conversion above 20 %. At ca. 65 % of NO_3^- conversion, this catalyst showed a selectivity to NH_4^+ of 50%, whereas the catalyst supported on AC showed 35 %. Pd-Cu/CNF and Pd-Cu/ENS350 catalysts exhibited equivalent selectivity to NH_4^+ (ca. 6 %), whereas Pd-Cu/ENS250 showed the lowest value: around 1 %. The activity of Pd-Cu/G was very low, reaching NO_3^- conversion values lower than 35 % and making difficult the comparison to other catalysts.

With the aim of further exploring the behavior of those catalysts supported on rGO, CNF, G at high NO_3^- conversion, catalytic runs with lower initial NO_3^- concentration (20 mg /

L) were performed (Figure 5b). NO_3^- conversion increased up to 85 % in the case of Pd-Cu/rGO catalyst and to 100 % in the case of Pd-Cu/G and Pd-Cu/CNF. When compared at 80-85 % of NO_3^- conversion, the selectivity to NH_4^+ was 50-55 %, 21 % and 5-7 % for the Pd-Cu/rGO, Pd-Cu/G and Pd-Cu/CNF catalysts, respectively. The selectivity to NH_4^+ is higher for the reactions at high nitrate concentration (Figure 5a), showing that competence among species for the active sites, probably from early stages of the experiment, can decrease the accumulation of intermediate N species. This effect can be observed from the lower increase of NH_4^+ at nearly complete NO_3^- conversion.

From the results in Figures 5a and 5b, it has to be noted that the three catalysts yielding lower selectivity to NH_4^+ are characterized by good conductivity of the support, and that two of them show the largest nanoparticle size (Pd-Cu/ENS250 and Pd/CNF). In this sense, Yoshinaga et al. [20] reported that selectivity to N_2 increased with Pd crystallite size since the Pd edges and corners have higher hydrogenation ability. They also indicated that the deposition of Cu atoms on Pd edges and corners could also avoid the formation of NH_4^+ , favoring the selectivity to N_2 . However, in the current work, one of the catalysts yielding low selectivity to NH_4^+ had also the smallest nanoparticle size (Pd-Cu/ENS350). Interestingly, ENS350 was one of the most conductive supports tested in this work. In the case of Pd-Cu/CNF catalyst, it has a highly conductive support and relatively large nanoparticle size among the tested. This catalyst only showed a significant increase of the selectivity to NH_4^+ at close to 100 % conversion, which can be related to the high H/N ratio occurring once the NO_3^- concentrations on the catalyst surface is very low, and uptaken intermediate N species evolve to NH_4^+ [23]. rGO is the less conductive of the supports tested and Pd-Cu/rGO catalyst showed the highest NH_4^+ formation. Li et al. [24] reported that charge transfer from metal to support can change the adsorption and activation of intermediate species on Ru/ TiO_2 catalysts in CO_2 hydrogenation, probably

due to the different extent of H₂ spill-over, affecting the selectivity. They observed a high activation of intermediate species in the cases where less charge transfer occurred, thus leading to deep hydrogenation to CH₄. On the contrary, higher charge transfer led to a weakening in adsorption and activation of the intermediates, favoring selectivity to CO. Rao et al. [25] reported that charge transfer not only takes place between noble metal and metal oxides supports, as they evidenced the influence on the selectivity of charge transfer between Pd and CNT support in the hydrogenation of cinnamaldehyde. Hydrogenation of C=O or C=C was effectively modulated by thermal treatment of the support at 1000 °C provoking a higher charge transfer. They also proposed that a decrease in the work function of the graphenic layer of the CNT, caused by oxygen surface functionalities disappearance by annealing, could increase the difference between the work function of Pd and CNT, affecting to charge distribution. Therefore, conductive supports such as carbon blacks, CNF or G allow charge transfer between metal and carbon supports to occur, affecting to the adsorption and activation of the intermediate N species, and hindering the overreduction of intermediate N species to NH₄⁺.

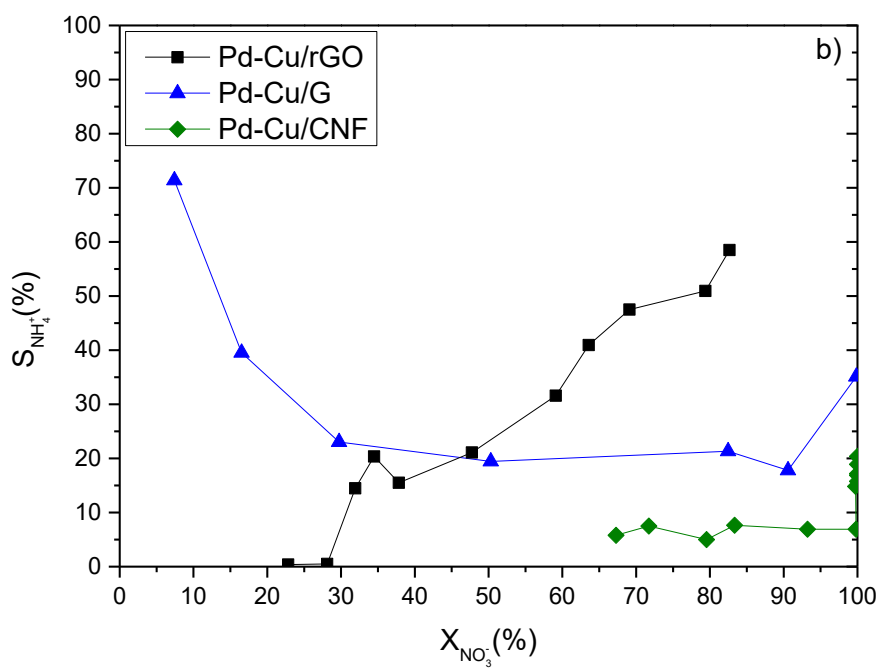
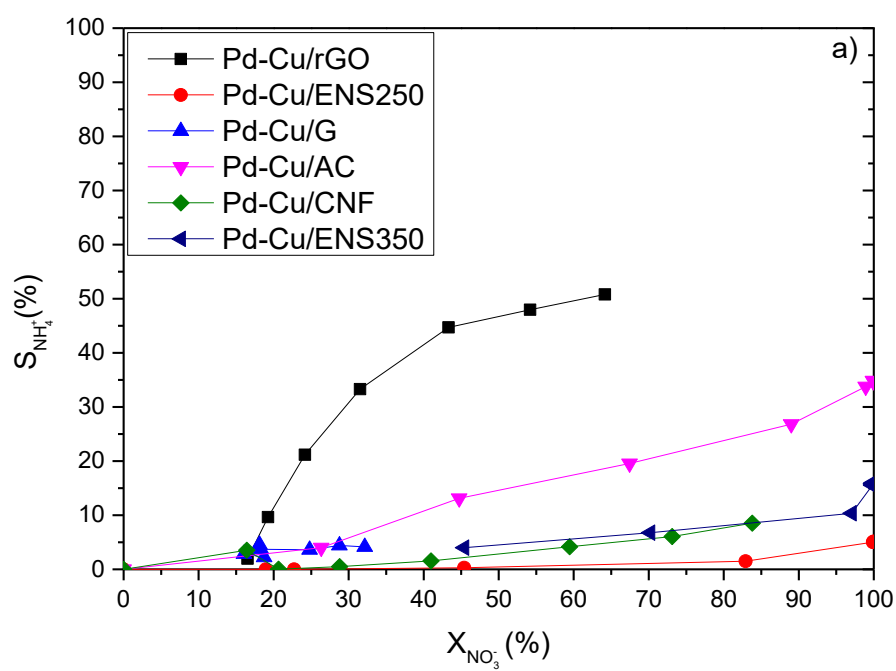


Figure 5. selectivity to NH_4^+ vs NO_3^- conversion a) $[\text{NO}_3^-]_0 = 100 \text{ mg/L}$ and b) $[\text{NO}_3^-]_0 = 20 \text{ mg/L}$ (H_2 flow: 50 N mL/min, CO_2 flow: 50 N mL/min, 0.4 g/L of catalyst)

3.3 Influence of H₂ availability on catalyst performance.

Figure 6 shows NO₃⁻ conversion vs time curves for Pd-Cu/rGO, Pd-Cu/CNF, Pd-Cu/ENS250 and Pd-Cu/ENS350 catalysts at different H₂ flow rates. In all the cases, the decrease in H₂ flow led to a decrease in NO₃⁻ conversion, being this effect especially pronounced for those catalysts with higher activity, i.e. Pd-Cu/ENS250 and Pd-Cu/ENS350. H₂ was bubbled into the reaction system together with CO₂, therefore a lower H₂ flow can be assumed to lead to lower H₂ partial pressure in the system, and in turn lower amount of H₂ available in the aqueous media for reduction reaction. In this conditions H₂ may become the limiting reagent because of its lower concentration and lower mass transfer rate.

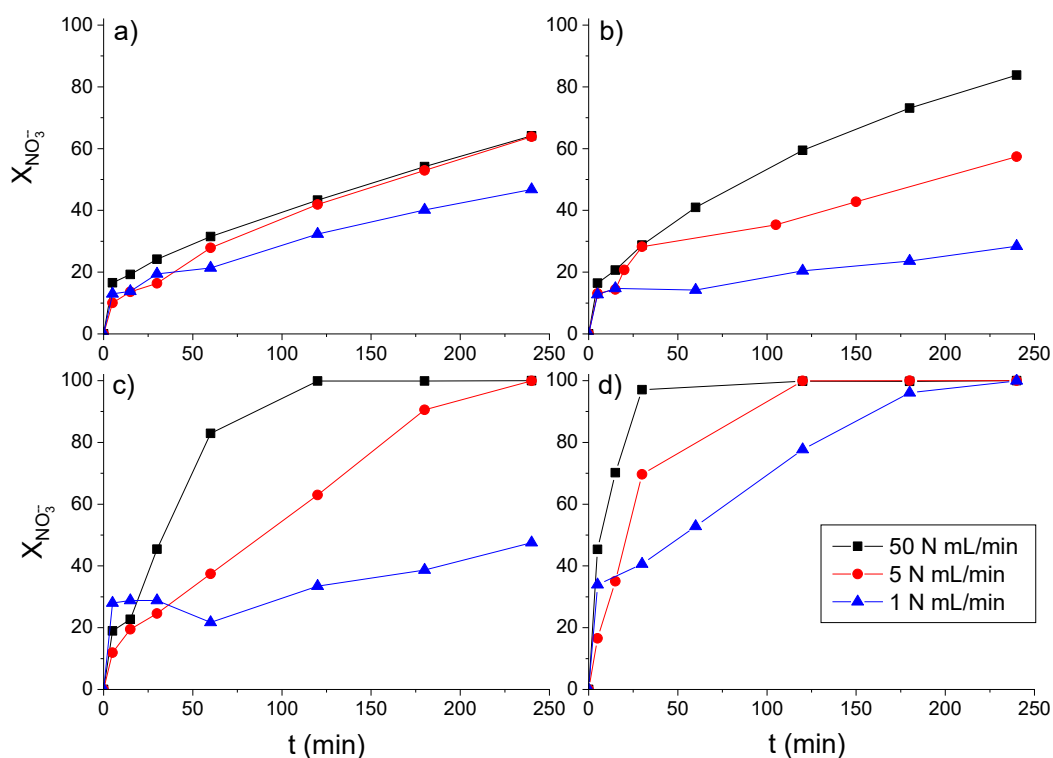


Figure 6. NO₃⁻ conversion upon reaction time for a) Pd-Cu/rGO; b) Pd-Cu/CNF; c) Pd-Cu/ENS250 and d) Pd-Cu/ENS350 at different H₂ flow ([NO₃⁻]₀ = 100 mg/L, CO₂ flow: 50 N mL/min, 0.4 g/L of catalyst)

Figure 7 shows the selectivity to NH_4^+ vs NO_3^- conversion curves for Pd-Cu/rGO, Pd-Cu/CNF, Pd-Cu/ENS250 and Pd-Cu/ENS350 catalysts at different H_2 flow rates. The decreasing H_2 flow resulted in a lower selectivity to NH_4^+ that can be more clearly observed in the case of Pd-Cu/rGO and Pd-Cu/ENS250 catalysts. This can be related to a lower H_2 availability that limits the H/N ratio and overreduction of intermediate N species at catalytic sites. In the case of Pd-Cu/CNF and Pd-Cu/ENS250 the differences in activity of these catalysts at different H_2 flows, hinders comparison at the 3 different flows tested. The release of NH_4^+ for nearly complete NO_3^- conversion was not suppressed, but in general lower release was observed in the test were the availability of H_2 was lower.

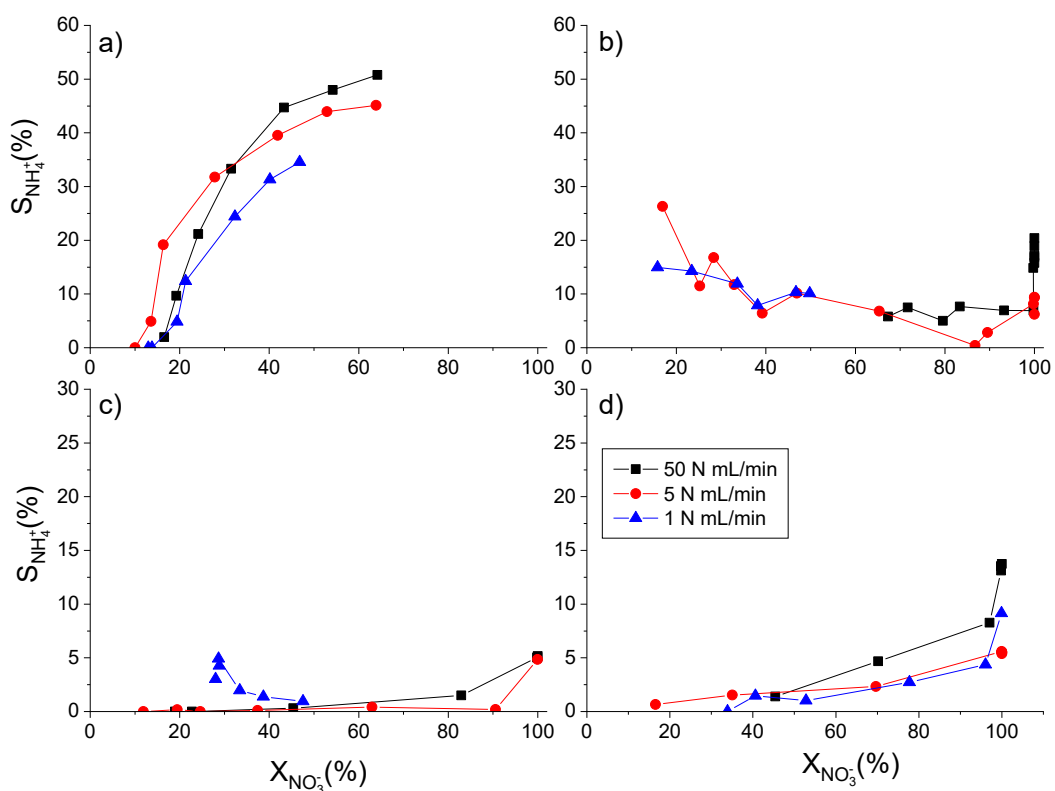


Figure 7. Selectivity to NH_4^+ vs NO_3^- conversion for a) Pd-Cu/rGO; b) Pd-Cu/NFC; c) Pd-Cu/ENS250 and d) Pd-Cu/ENS350 at different H_2 flows. $[\text{NO}_3^-]_0 = 100 \text{ mg/L}$

3.3.1 Mass transfer regime study

Table 3 shows the calculated Ca_{G-L} , Ca_{L-S} , $(\Phi_s)_{H_2}$, and $(\Phi_s)_{NO_3^-}$ values for the reactions carried out with Pd-Cu/rGO, Pd-Cu/CNF, Pd-Cu/ENS250, and Pd-Cu/ENS350 catalysts at different H_2 flows. According to Ca_{G-L} values, mass transfer limitations cannot be ruled out for any of the catalysts when tested at the lowest H_2 flow (1 N mL/min). Likewise, mass transfer cannot be ruled either for Pd-Cu/ENS250 and Pd-Cu/ENS350 catalysts at a H_2 flow of 5 N mL/min. It must be noted that some authors used a more restrictive criterion ($Ca < 0.05$) to discard mass transfer limitations [26, 27]. According to this last, mass transfer limitations could not be ruled out at ≤ 5 N mL/min of H_2 flow for any of the catalysts. Moreover, the Ca_{G-L} values for Pd-Cu/ENS250 and Pd-Cu/ENS350 catalysts were under but quite close to the limit (0.034-0.041) at 50 N mL/min flow. These results are in good agreement with the trends observed for the activity (Fig. 6) and the selectivity to NH_4^+ (Fig. 7), where lower values of activity and selectivity can be observed for the experiments where lower H_2 flows were used. The change in selectivity was evident even for Pd-Cu/rGO, whose activity did not decay so drastically with decreasing H_2 flow. In the case of Ca_{L-S} and Weisz-Prater modules, values were low enough to rule out mass transfer or intraparticle diffusion limitations. Therefore, changes in the behavior of the catalysts can be ascribed to external mass transfer.

Table 3. Ca_{G-L} , Ca_{L-S} , $(\Phi_s)_{H_2}$, and $(\Phi_s)_{NO_3^-}$ at different H_2 flows for Pd-Cu/rGO, Pd-Cu/CNF, Pd-Cu/ENS250, and Pd-Cu/ENS350 catalysts

Catalyst	H_2 flow (N mL/min)	Ca_{G-L} ($\cdot 10^{-2}$)	$Ca_{L-S}H_2$ ($\cdot 10^{-6}$)	$Ca_{L-S}NO_3^-$ ($\cdot 10^{-7}$)	$(\Phi_s)_{H_2}$ ($\cdot 10^{-4}$)	$(\Phi_s)_{NO_3^-}$ ($\cdot 10^{-4}$)
Pd-Cu/rGO	50	1.0	0.3	0.9	2.0	0.7
	5	9.1	1.3	0.7	9.1	0.6
	1	43	3.8	0.5	28	0.4
Pd-Cu/CNF	50	1.5	0.4	5.9	2.7	4.9
	5	5.1	0.7	2.0	5.1	1.7
	1	9.5	0.8	0.5	6.1	0.4
Pd-Cu/ENS250	50	3.4	0.9	2.8	6.5	2.3
	5	13	1.8	1.0	13	0.8
	1	44	3.9	0.5	29	0.4
Pd-Cu/ENS350	50	4.1	1.1	3.4	7.8	2.8
	5	45	6.2	3.5	45	2.9
	1	154	14	1.7	99	1.4

4. Conclusions

The use of carbon materials with different structure as catalyst supports allows bimetallic Pd-Cu catalysts to achieve different behavior in terms of NO_3^- conversion and selectivity to NH_4^+ . Catalysts supported on carbon materials with high specific surface area showed nearly complete NO_3^- conversion. This behavior can be linked to better dispersion of the metallic phase, but catalysts supported on ENS250 carbon black showed relatively high activity in spite of their relatively low specific surface and large size of metallic nanoparticles, suggesting that conductivity of the support also could contribute to NO_3^- conversion. Catalysts with supports of relatively high or moderate conductivity, showed lower selectivity to NH_4^+ , especially in the case of carbon blacks (ENS250 and ENS350) and CNF, which can be ascribed to charge transfer from metal to support. When H_2 flow was reduced in the catalytic runs, NO_3^- conversion and selectivity to NH_4^+ also diminished, suggesting that mass transfer limitation can occur at low H_2 flows. The analysis of the parameters describing mass transfer revealed external gas-liquid mass transfer limitations for H_2 . Ca_{G-L} values above 0.05 (limiting value) were achieved when

H₂ flow of 1 and 5 N mL/min were used, which in turn resulted in a decay in NO₃⁻ conversion and selectivity to NH₄⁺. The results obtained indicate that approaches based on the control of mass transfer can be useful to control selectivity to NH₄⁺, and combination with catalysts properties such as conductivity of the supports makes possible additional control.

Acknowledgements

The authors greatly appreciate the support from Spanish Agencia Estatal de Investigación (AEI, RTI2018-098431-BI00). Dydia Tanisha González thanks the Regional Government of Madrid a research grant (PEJ-2020-AI/AMB-17551) and Adrián Marí thanks the Spanish AEI a research grant (PRE-2019-088601).

References

- [1] K. Vorlop, T. Tacke, Erste Schritte auf dem Weg zur edelmetallkatalysierten Nitrat- und Nitrit-Entfernung aus Trinkwasser, Chem. Ing. Tech. 61 (1989) 836-837. <https://doi.org/10.1002/cite.330611023>
- [2] J. Martínez, A. Ortiz, I. Ortiz, State-of-the-art and perspectives of the catalytic and electrocatalytic reduction of aqueous nitrates, Appl. Catal. B: Env. 207 (2017) 42-59. <https://doi.org/10.1016/j.apcatb.2017.02.016>.
- [3]. Council Directive 98/83/EC of 3 November 1998 on the quality of water intended for human consumption, ANNEX I: PARAMETERS AND PARAMETRIC VALUES, PART B: Chemical parameters. EUR-Lex. Retrieved 11th May 2021. <https://eur-lex.europa.eu/legal-content/EN/TXT/HTML/?uri=CELEX:31998L0083&from=EN>.
- [4] N. Barrabés, J. Sá, Catalytic nitrate removal from water, past, present and future perspectives, Appl. Catal. B: Env. 104 (2011) 1-5. <https://doi.org/10.1016/j.apcatb.2011.03.011>
- [5] O.S.G.P. Soares, J.J.M. Órfão, M.F.R. Pereira, Nitrate reduction in water catalysed by Pd-Cu on different supports, Desalination 279 (2011) 367-374. <https://doi.org/10.1016/j.desal.2011.06.037>.

- 443 [6] A.S. Santos, J. Restivo, C.A. Orge, M.F. Pereira, O.S. Soares, Nitrate Catalytic
444 Reduction over Bimetallic Catalysts: Catalyst Optimization, *C* 6(4) (2020) 78.
445 <https://doi.org/10.3390/c6040078>.
- 446 [7] R.S. Postma, R. Brunet Espinosa, L. Lefferts, Competitive Adsorption of Nitrite and
447 Hydrogen on Palladium during Nitrite Hydrogenation, *ChemCatChem* 10 (2018) 3770-
448 3776. <https://doi.org/10.1002/cctc.201800523>.
- 449 [8] J.A. Baeza, F. García-Missana, A.S. Oliveira, L. Calvo, M.A. Gilarranz, Influence of
450 H₂ availability in the catalytic reduction of nitrates in fixed bed reactors, *Chem. Eng.*
451 *Sci.*, (2021) 116887. <https://doi.org/10.1016/j.ces.2021.116887>
- 452 [9] H. Yagi, F. Yoshida, Gas Absorption by Newtonian and Non-Newtonian Fluids in
453 Sparged Agitated Vessels, *Ind. Eng. Chem. Proc. Des. Dev.* 14 (1975) 488-493.
454 <https://doi.org/10.1021/i260056a024>
- 455 [10] K. Miyabe, R. Isogai, Estimation of molecular diffusivity in liquid phase systems
456 by the Wilke–Chang equation, *J. Chromatogr., A* 1218 (2011) 6639-6645.
457 <https://doi.org/10.1016/j.chroma.2011.07.018>
- 458 [11] W. Ranz, W. Marshall, Evaporation from drops, *Chem. Eng. Prog.* 48 (1952) 141-
459 146.
- 460 [12] H.H. Lee, *Heterogeneous reactor design*; Sponser Org., Butterworth Publishers,
461 Stoneham, MA, United States, 1984.
- 462 [13] B. P. Chaplin, E. Roundy, K. A. Guy, J. R. Shapley, C. J. Werth. Effects of Natural
463 Water Ions and Humic Acid on Catalytic Nitrate Reduction Kinetics Using an Alumina
464 Supported Pd–Cu Catalyst. *Environ. Sci. Technol.* 2006, 40, 9, 3075.
465 <https://doi.org/10.1021/es0525298>
- 466
467 [14] F.A. Marchesini, G. Mendow, N.P. Picard, F.M. Zoppas, V.S. Aghemo, L.B.
468 Gutierrez, C.A. Querini, E E. Miró. PdIn Catalysts in a Continuous Fixed Bed Reactor
469 for the Nitrate Removal from Groundwater *Int. J. Chem. React. Eng.* 2019, 20180126.
470 <https://doi.org/10.1515/ijcre-2018-0126>
- 471 [15] P. Granger, S.Tronc  a, J.P. Dacquin, M. Trentesaux, O. Gardoll, N.Nuns,
472 V.I.Parvulescu. Peculiar kinetic properties of Cu-doped Pd/Ce_xZr_{1-x}O₂ in water
473 denitrification: Impact of Pd-Cu interaction vs structural properties of Ce_xZr_{1-x}O₂. *Appl.*
474 *Catal. B: Env.* 2019, 253, 391. <https://doi.org/10.1016/j.apcatb.2019.04.010>
- 475 [16] J. B. Butt, *Reaction Kinetics and Reactor Design*, second edition ed., CRC Press,
476 New York, 2000.
- 477 [17] X. Jiao, Y. Qiu, L. Zhang, X. Zhang, Comparison of the characteristic properties of
478 reduced graphene oxides synthesized from natural graphites with different
479 graphitization degrees, *RSC Adv.* 7 (2017) 52337-52344.
480 <https://doi.org/10.1039/C7RA10809E>

- 481 [18] T. Qiu, J. Yang, X. Bai, Y. Wang, The preparation of synthetic graphite materials
482 with hierarchical pores from lignite by one-step impregnation and their characterization
483 as dye absorbents, *RSC Adv.* 9 (2019) 12737-12746.
484 <https://doi.org/10.1039/C9RA00343F>
- 485 [19] M. Al Bahri, L. Calvo, M.A. Gilarranz, J.J. Rodriguez, F. Epron, Activated carbon
486 supported metal catalysts for reduction of nitrate in water with high selectivity towards
487 N₂, *Appl. Catal. B: Env.* 138-139 (2013) 141-148.
488 <https://doi.org/10.1016/j.apcatb.2013.02.048>
- 489 [20] Y. Yoshinaga, T. Akita, I. Mikami, T. Okuhara, Hydrogenation of Nitrate in Water
490 to Nitrogen over Pd–Cu Supported on Active Carbon, *J. Catal.* 207 (2002) 37-45.
491 <https://doi.org/10.1006/jcat.2002.3529>.
- 492 [21] K. Shafqat, S. Pitkäaho, M. Tiainen, L. Matějová, R.L. Keiski, Effect of
493 Nanoparticle Size in Pt/SiO₂ Catalyzed Nitrate Reduction in Liquid Phase,
494 *Nanomaterials* 11 (2021) <https://doi.org/10.3390/nano11010195>.
- 495 [22] F. Papa, I. Balint, C. Negrila, E. Olaru, I. Zgura, C. Bradu, Supported Pd–Cu
496 Nanoparticles for Water Phase Reduction of Nitrates. Influence of the Support and of
497 the pH Conditions, *Ind. Eng. Chem. Res.* 53 (2014) 19094-19103.
498 <https://doi.org/10.1021/ie503070f>.
- 499 [23] S.D. Ebbesen, B.L. Mojet, L. Lefferts, In situ ATR-IR study of nitrite
500 hydrogenation over Pd/Al₂O₃, *J. Catal.* 256 (2008) 15-23.
501 <https://doi.org/10.1016/j.jcat.2008.02.013>
- 502 [24] X. Li, J. Lin, L. Li, Y. Huang, X. Pan, S.E. Collins, Y. Ren, Y. Su, L. Kang, X.
503 Liu, Y. Zhou, H. Wang, A. Wang, B. Qiao, X. Wang, T. Zhang, Controlling CO₂
504 Hydrogenation Selectivity by Metal-Supported Electron Transfer, *Angew. Chem. Int.*
505 *Ed.* 59 (2020) 19983-19989. <https://doi.org/10.1002/anie.202003847>
- 506 [25] R.G. Rao, R. Blume, T.W. Hansen, E. Fuentes, K. Dreyer, S. Moldovan, O. Ersen,
507 D.D. Hibbitts, Y.J. Chabal, R. Schlögl, J. Tessonier, Interfacial charge distributions in
508 carbon-supported palladium catalysts, *Nat. Commun.* 8 (2017) 340.
509 <https://doi.org/10.1038/s41467-017-00421-x>
- 510 [26] L. Ronchin, L. Toniolo, Selective hydrogenation of benzene to cyclohexene using a
511 suspended Ru catalyst in a mechanically agitated tetraphase reactor, *Catal. Today* 48
512 (1999) 255-264. [https://doi.org/10.1016/S0920-5861\(98\)00380-0](https://doi.org/10.1016/S0920-5861(98)00380-0)
- 513 [27] J. Dam, A. Ramanathan, K. Djanashvili, F. Kapteijn, U. Hanefeld, Synthesis,
514 characterization and performance of bifunctional catalysts for the synthesis of menthol
515 from citronellal, *RSC Adv.* 7 (2017) 12041-12053.
516 <https://doi.org/10.1039/C6RA25931F>